http://dx.doi.org/10.21611/qirt.2012.399

Thermal diffusivity measurements as a non destructive tool for the microstructural characterisation and the integrity assessment of thermal barrier coatings

Federico Cernuschi

Power Generation Systems Dep.
Ricerca sul Sistema Energetico – RSE S.p.A.
Via Rubattino, 54 - 20134 Milano - I

http://dx.doi.org/10.21611/qirt.2012.399

Acknowledgments

Paolo Bison

Igor Golosnoy

This work has been partially financed by the Research Fund for the Italian Electrical System under the Contract Agreement between RSE (formerly known as ERSE) and the Ministry of Economic Development - General Directorate for Nuclear Energy, Renewable Energy and Energy Efficiency stipulated on July 29, 2009 in compliance with the Decree of March 19, 2009

http://dx.doi.org/10.21611/qirt.2012.399

Summary

- Introduction to Thermal Barrier coatings (TBCs)

- Integrity assessment of TBC by thermal diffusivity evaluation

- Microstructural characterisation of TBC by thermal diffusivity evaluation and sintering forecasts

- Through-the-thickness and in-plane thermal diffusivity measurements

http://dx.doi.org/10.21611/qirt.2012.399

The gas turbine

http://dx.doi.org/10.21611/qirt.2012.399

GT Inlet Temperature / GT Efficiency

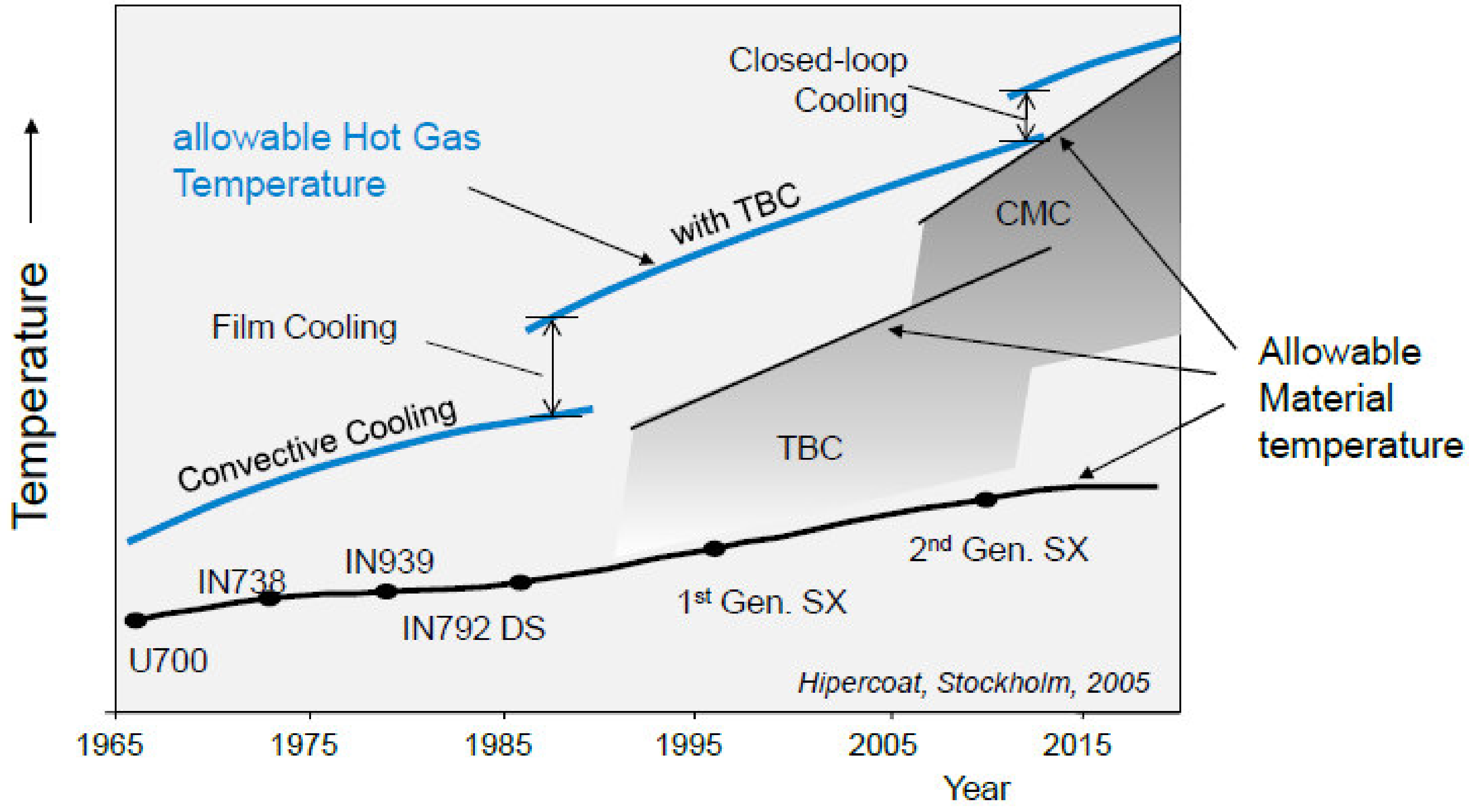

http://dx.doi.org/10.21611/qirt.2012.399

The GT hot path components

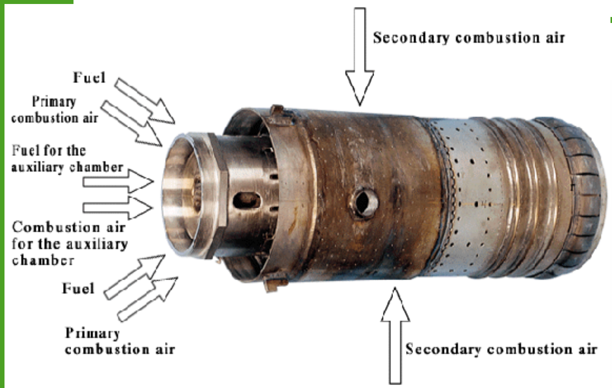

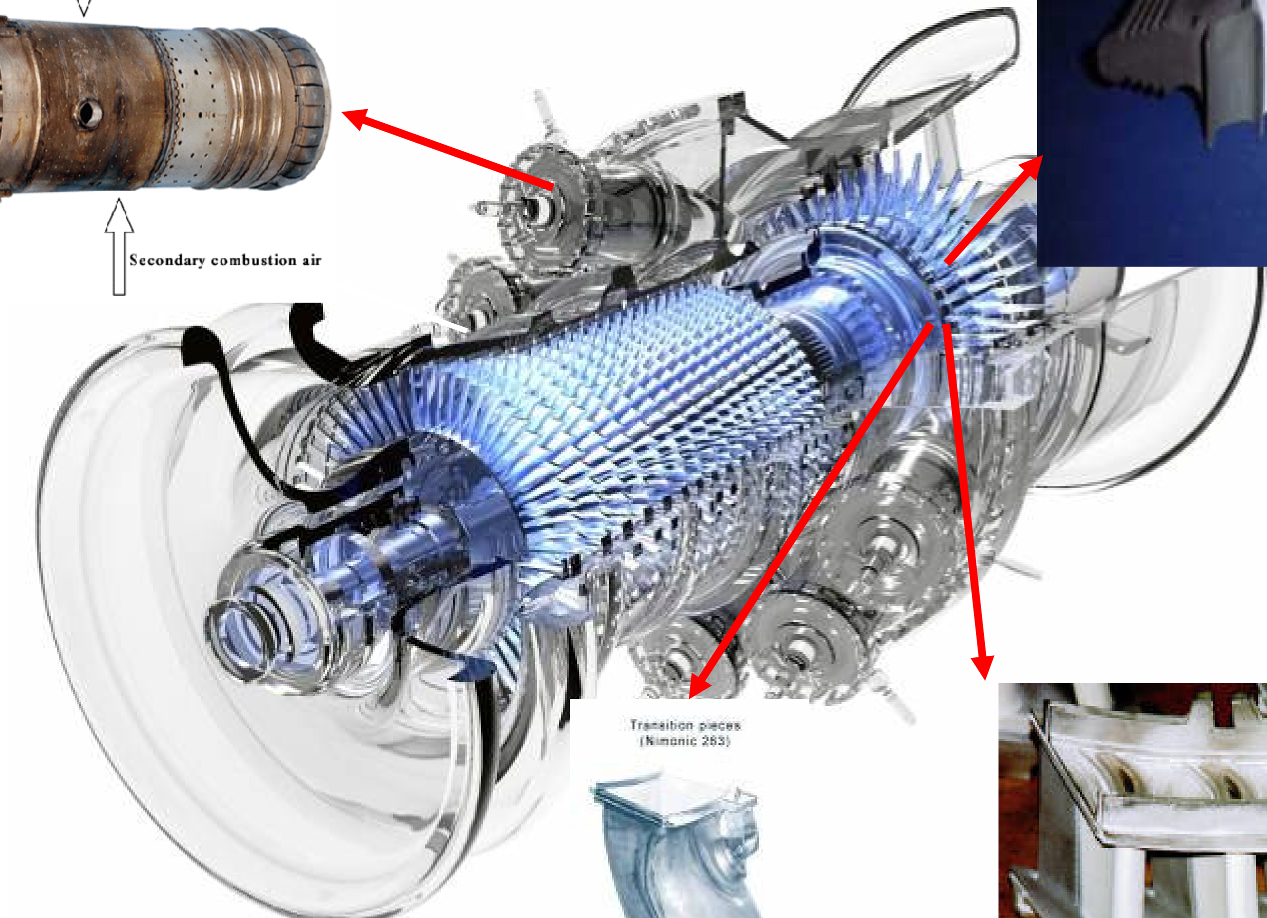

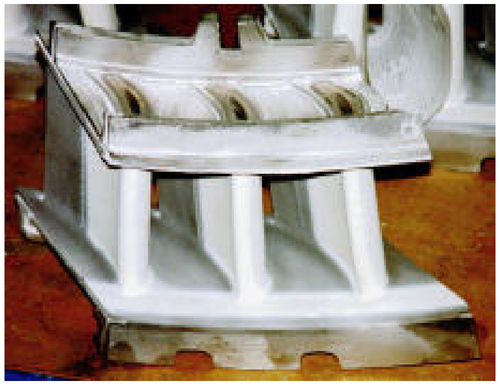

http://dx.doi.org/10.21611/qirt.2012.399

The thermal barrier coating (TBC)

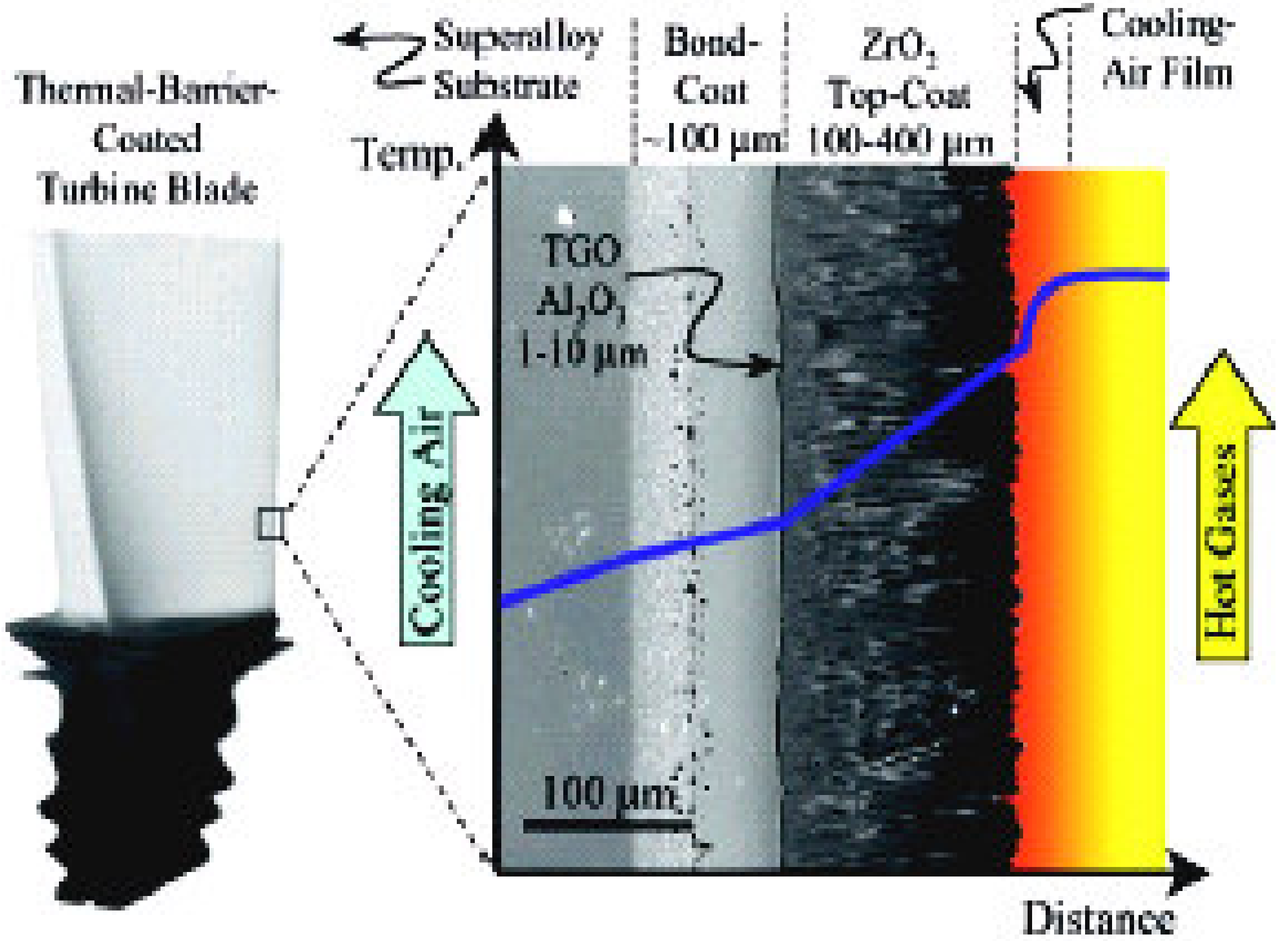

http://dx.doi.org/10.21611/qirt.2012.399

The material $8\% Y_2O_3+ZrO_2$

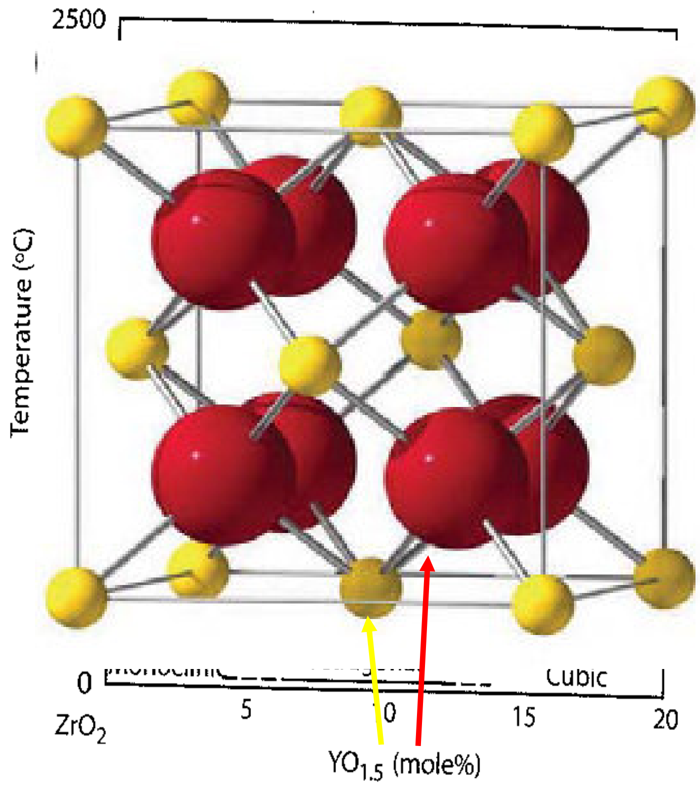

Fluoritic AO_2

A +4

- Maximum operating temperature 1200 °C
- TEC similar to that of substrate ($1*10^{-5}$ vs. $1.2 – 1.3 * 10^{-5}$)
- High toughness K_{1c} (9.5 – 10.5 Mpa $m^{1/2}$)
- Low thermal conductivity (2.8 – 2.2 W/mK)
- Coating ~1W/mK ⇦⇨50-170°C
- Coating thickness 100-1000 μm

http://dx.doi.org/10.21611/qirt.2012.399

The material $8\%Y_2O_3+ZrO_2$

$$\kappa = \frac{1}{3} C_v v \Lambda$$

$$\Lambda \cong d_i$$

$$Y^{+3} \rightarrow Zr^{+4} \rightarrow d_i \downarrow$$

Non phonon vibrational modes with $v<v_{sound}$

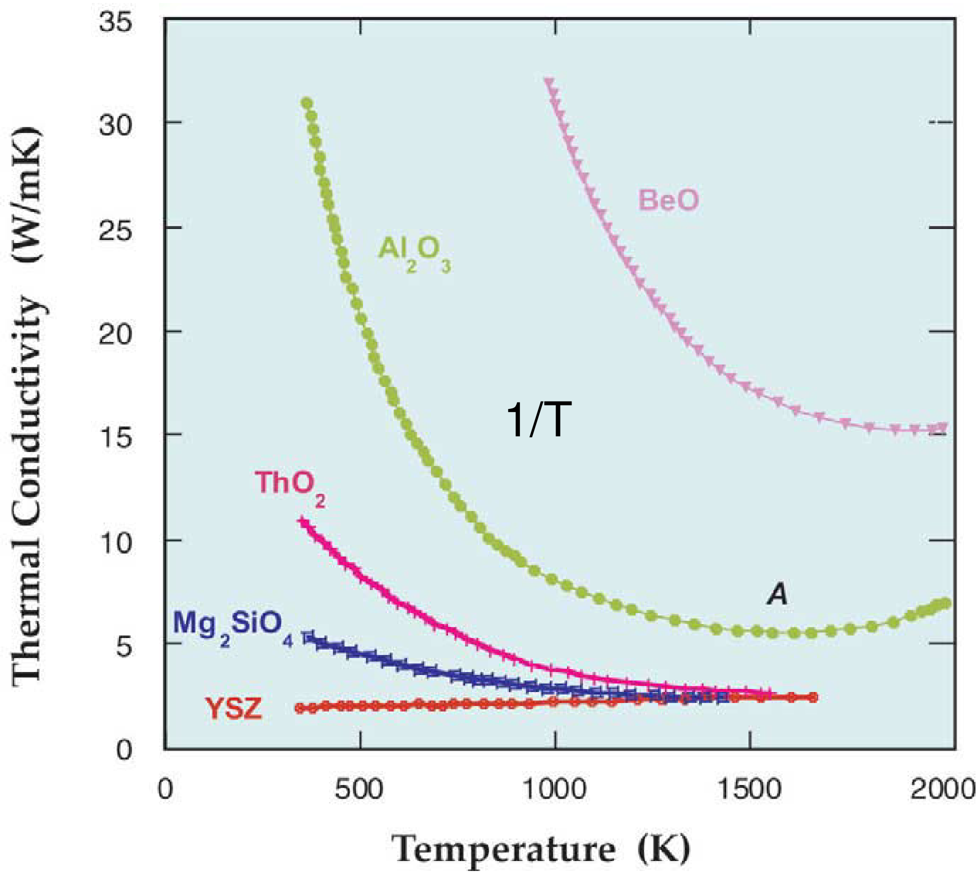

http://dx.doi.org/10.21611/qirt.2012.399

The deposition techniques: APS

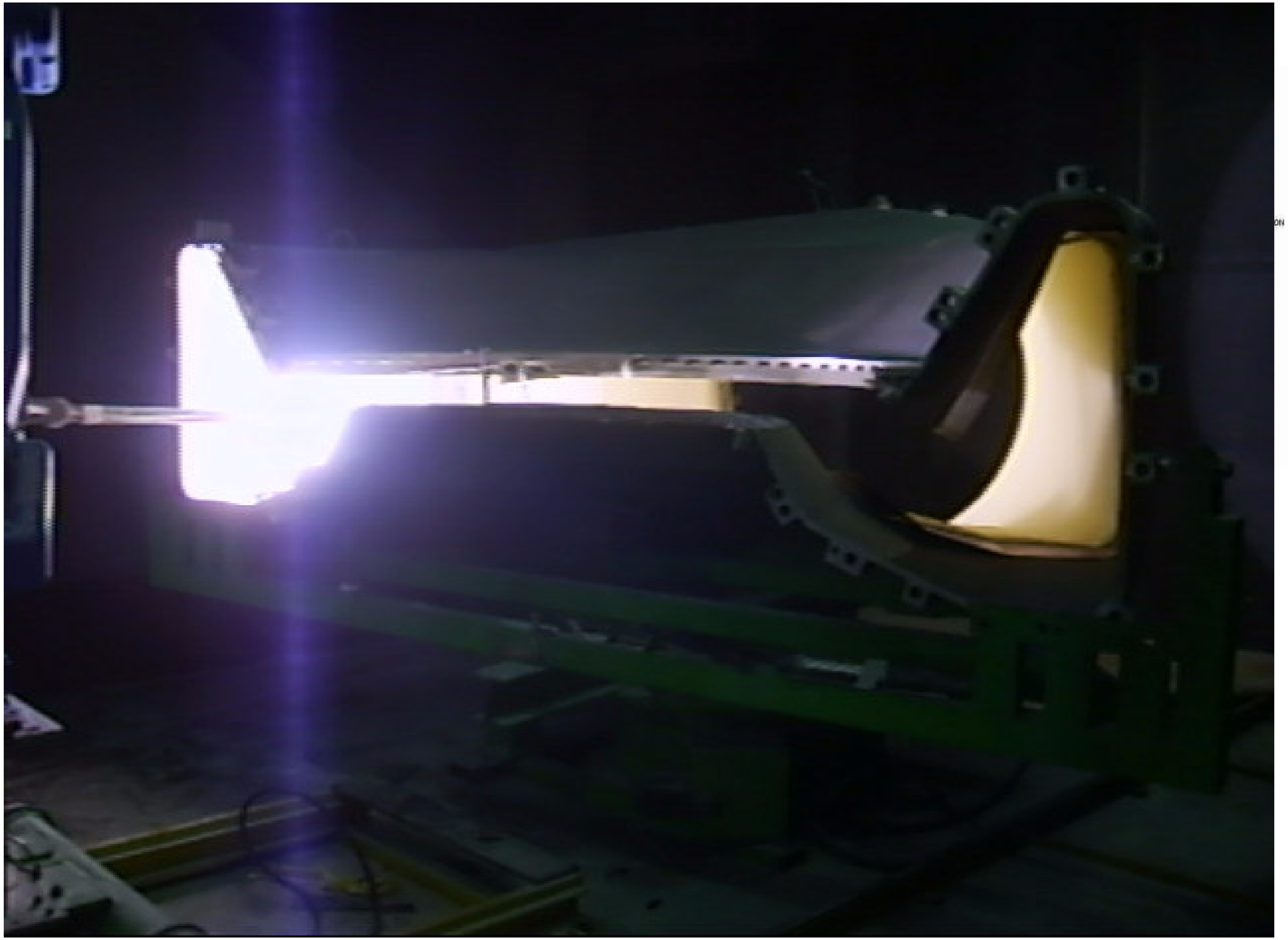

http://dx.doi.org/10.21611/qirt.2012.399

The deposition techniques: APS

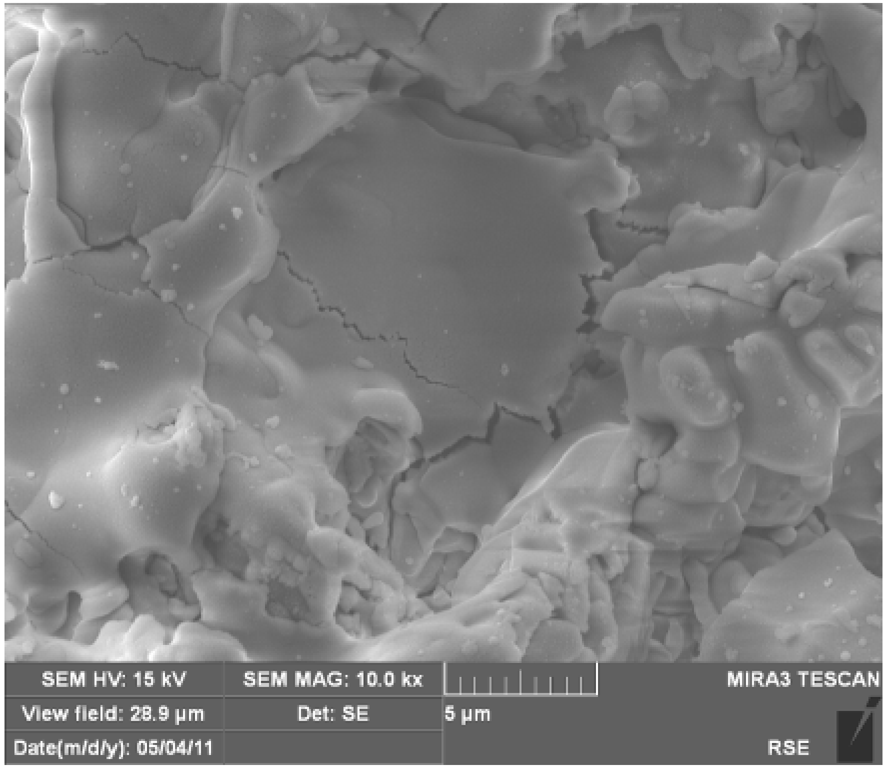

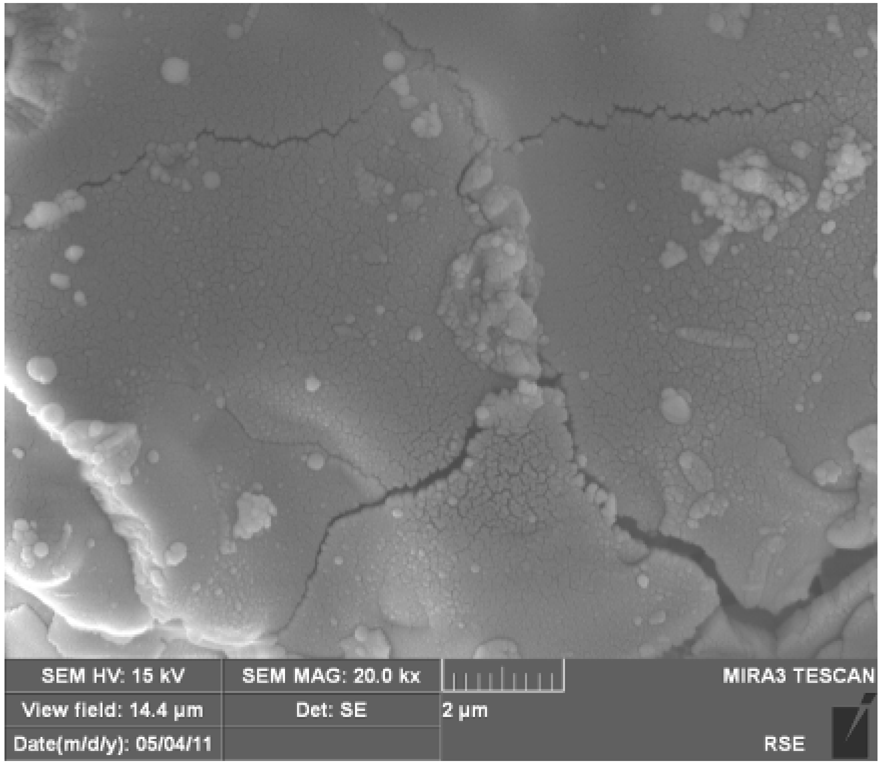

http://dx.doi.org/10.21611/qirt.2012.399

The deposition techniques: APS

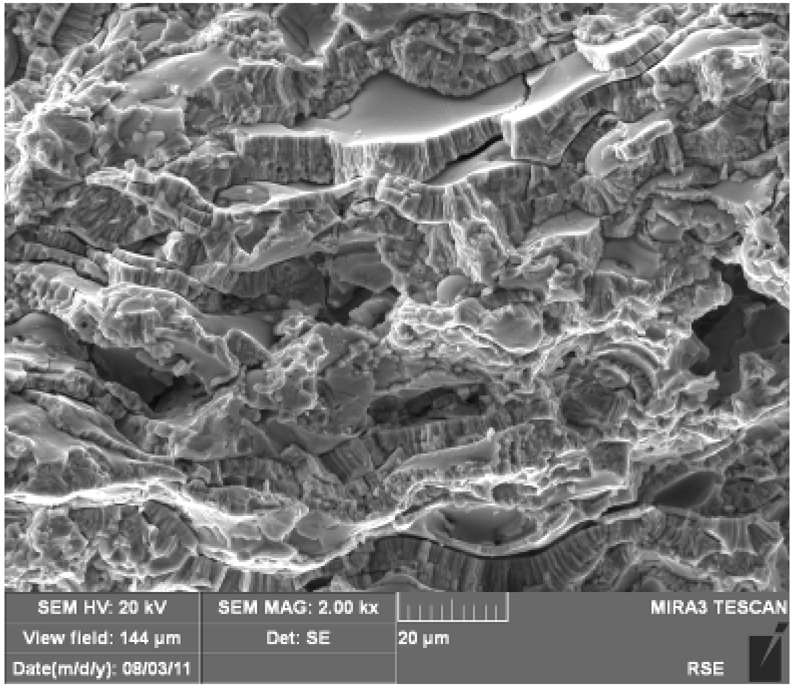

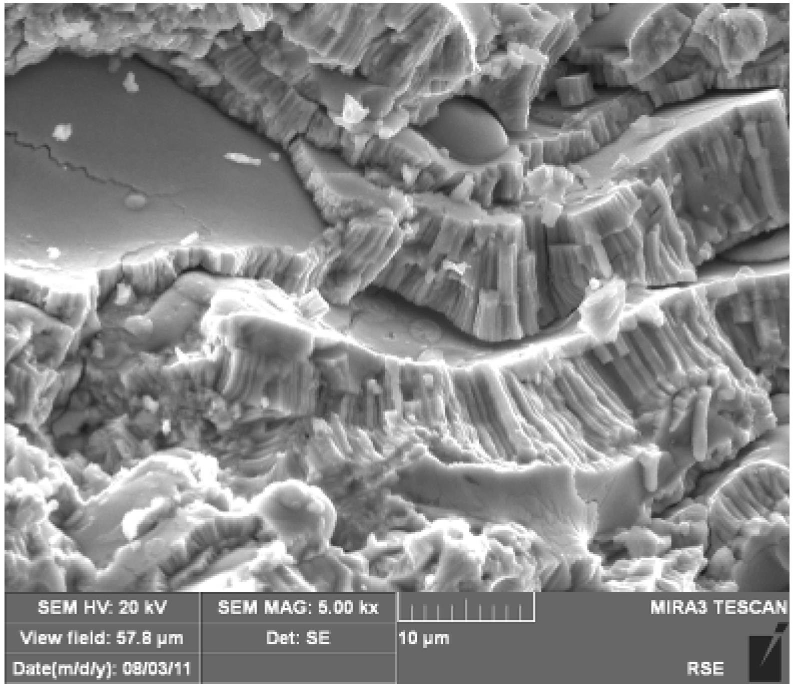

http://dx.doi.org/10.21611/qirt.2012.399

The deposition techniques: EBPVD

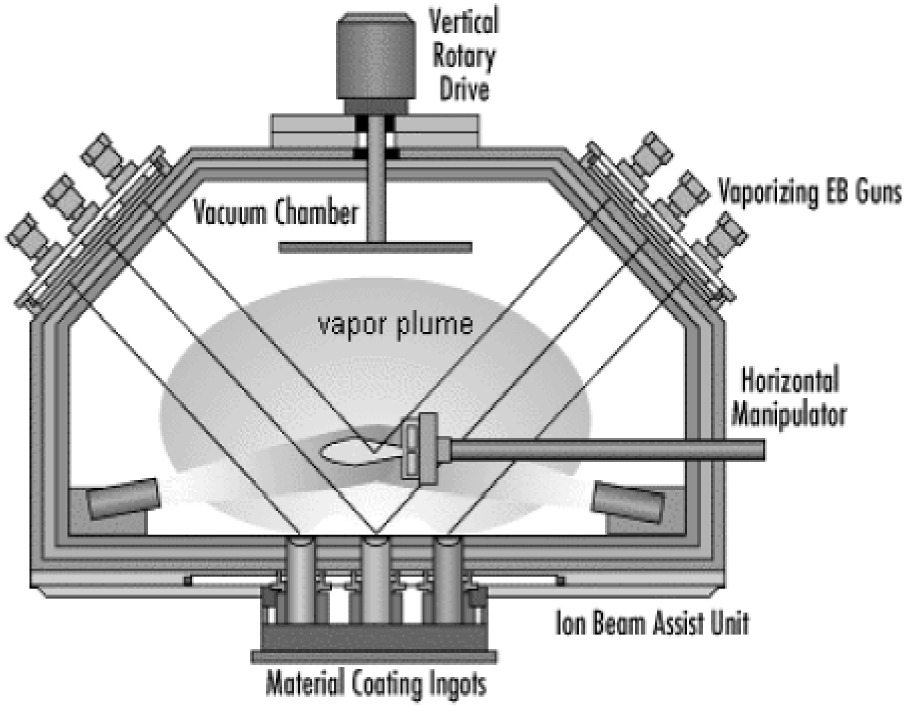

http://dx.doi.org/10.21611/qirt.2012.399

The deposition techniques: EBPVD

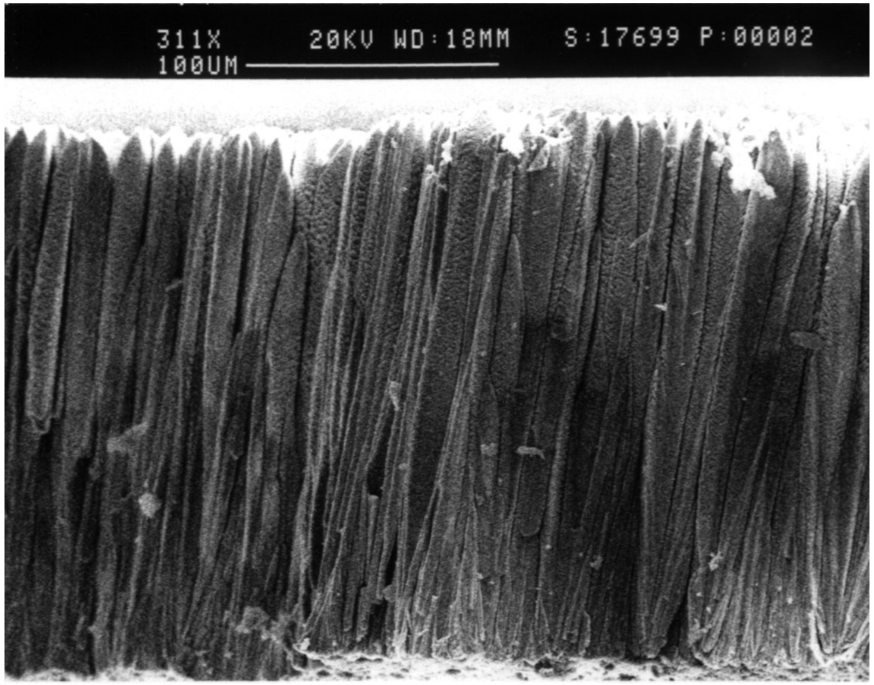

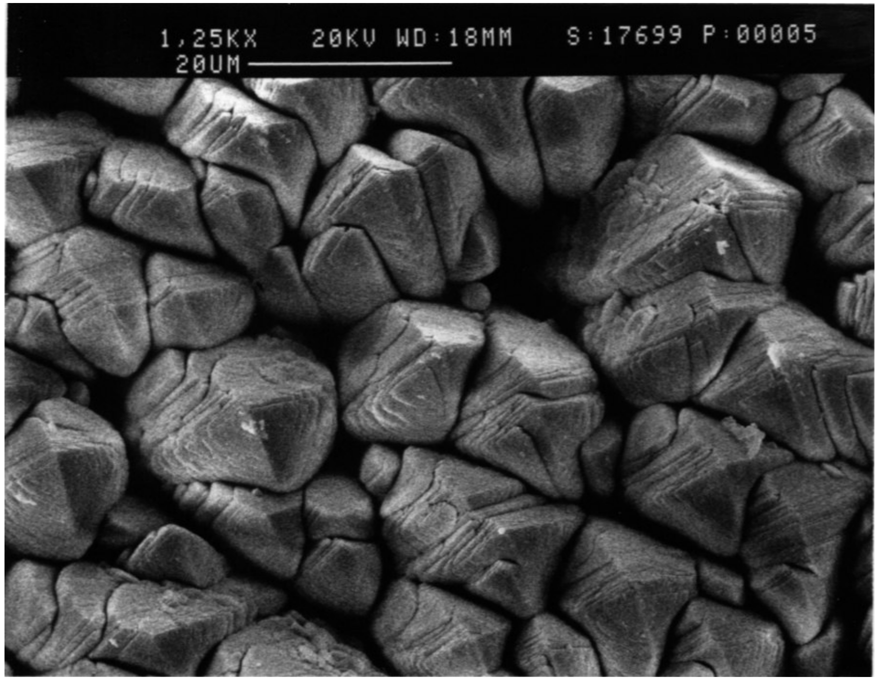

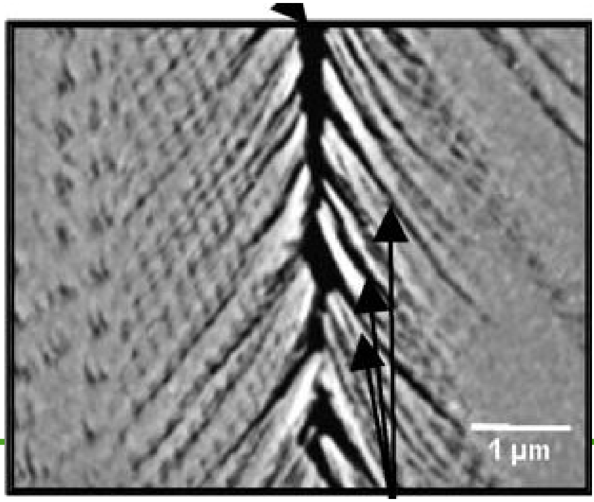

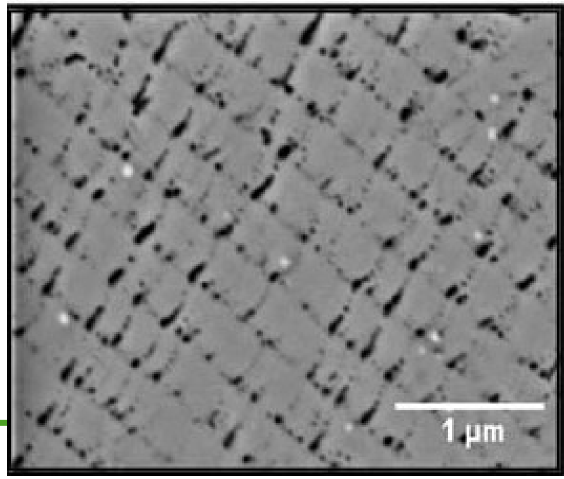

http://dx.doi.org/10.21611/qirt.2012.399

Failure mechanisms of TBC

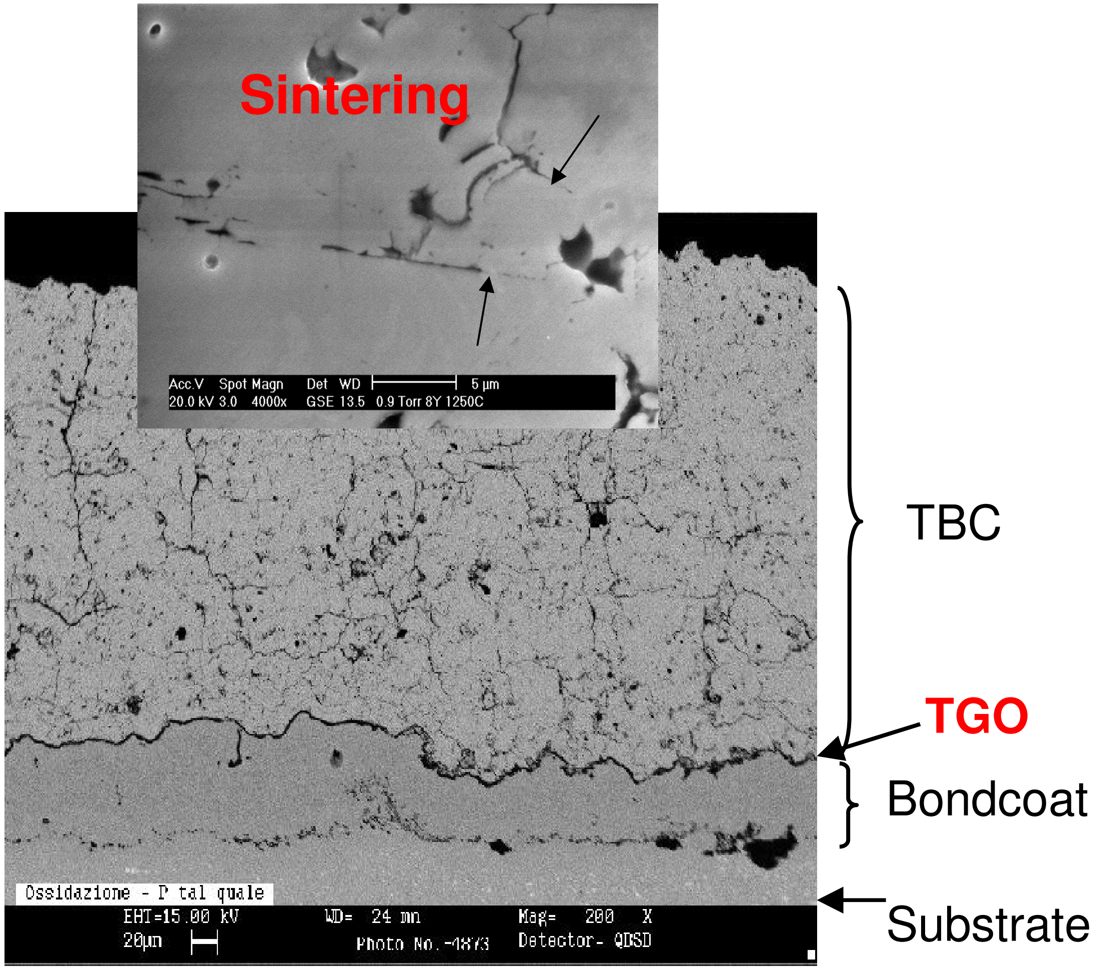

http://dx.doi.org/10.21611/qirt.2012.399

Failure mechanisms of TBC

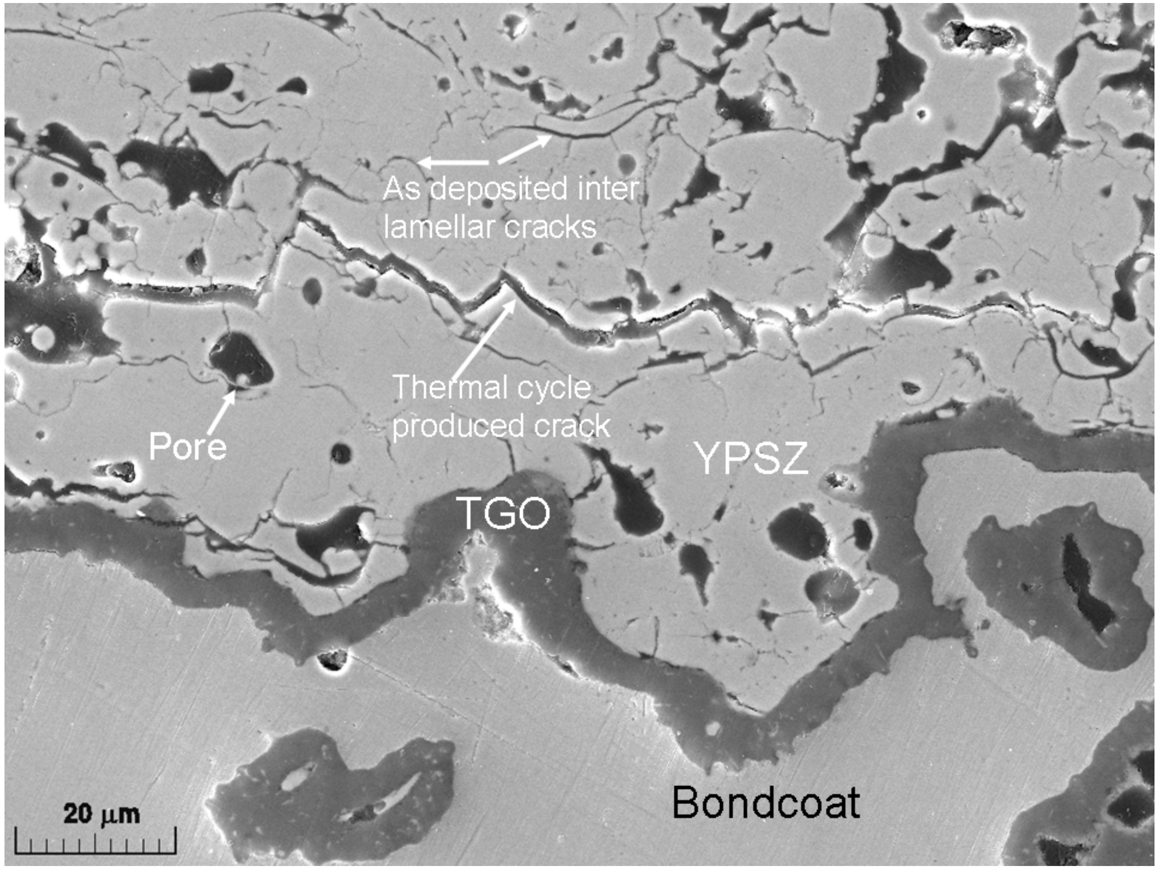

- TGO growth
- Thermal fatigue

http://dx.doi.org/10.21611/qirt.2012.399

Non destructive integrity assessment of TBCs Coupons

F. Cernuschi, S. Capelli, P. Bison, S. Marinetti, L. Lorenzoni, E. Campagnoli and C. Giolli, Acta Materialia 59 (2011) 6351–6361

http://dx.doi.org/10.21611/qirt.2012.399

ND detection of cracking at interface BC – TBC

The objective is to non destructively detect diffuse cracking at the interface between BC and TBC in coupons tested under cyclic oxidation

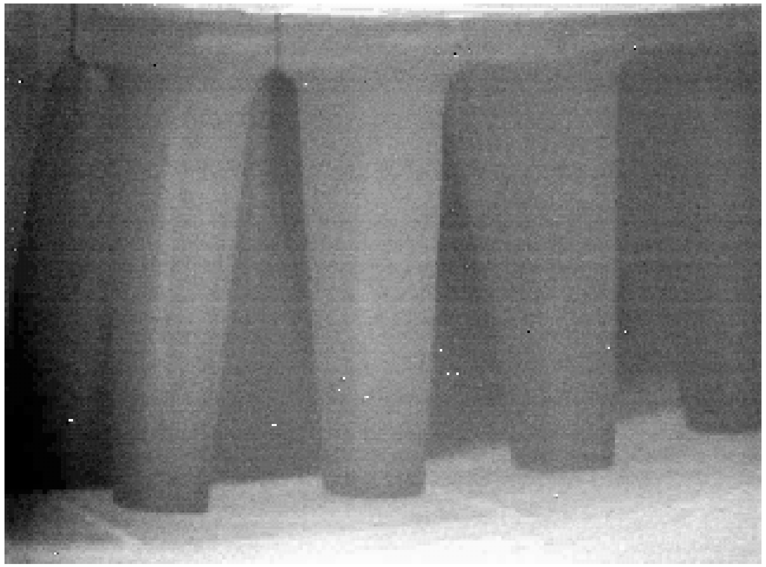

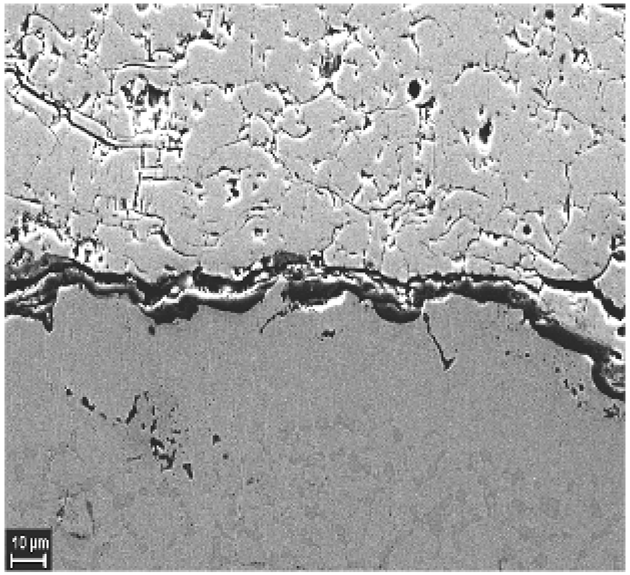

http://dx.doi.org/10.21611/qirt.2012.399

Ageing of TBC:sintering

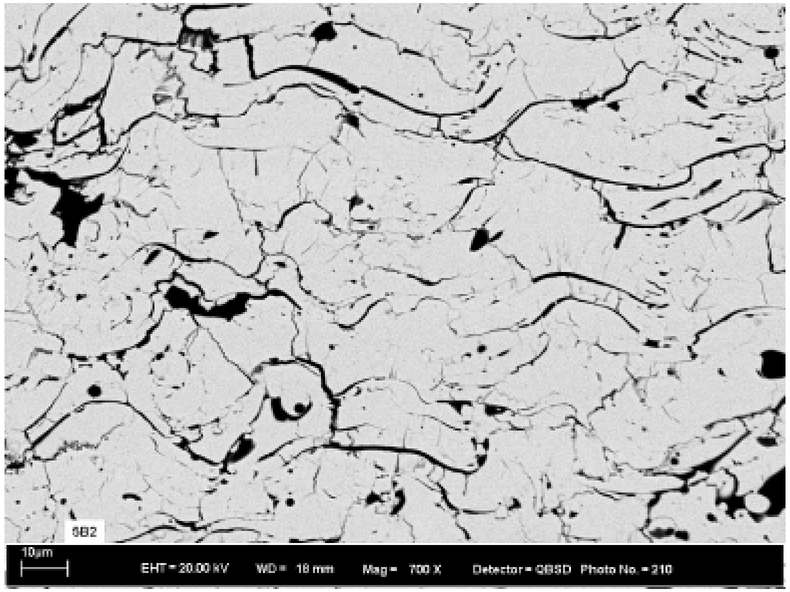

(T,t)

⇨

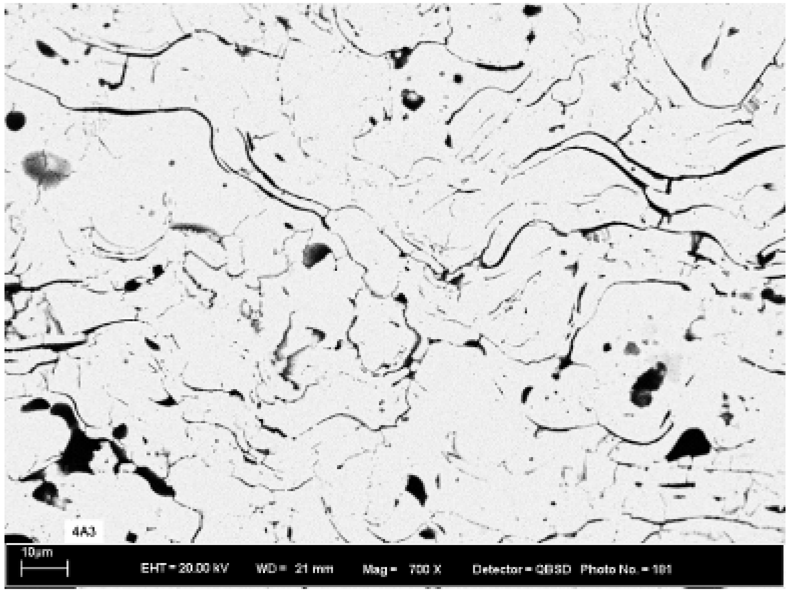

$(\alpha_0, E_0, H_0, \varphi_0, \ldots)$ ⇨ $(\alpha, E, H, \varphi \ \ldots) > (\alpha_0, E_0, H_0, \ldots)$

http://dx.doi.org/10.21611/qirt.2012.399

Ageing of TBC:cracking at the interface

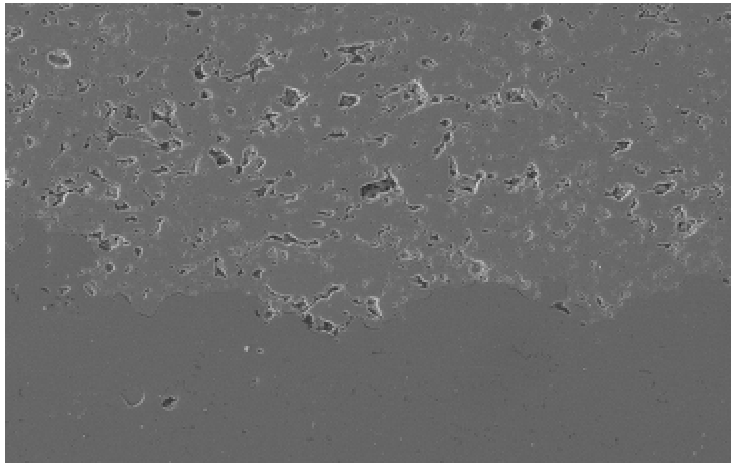

(T,t)

⇨

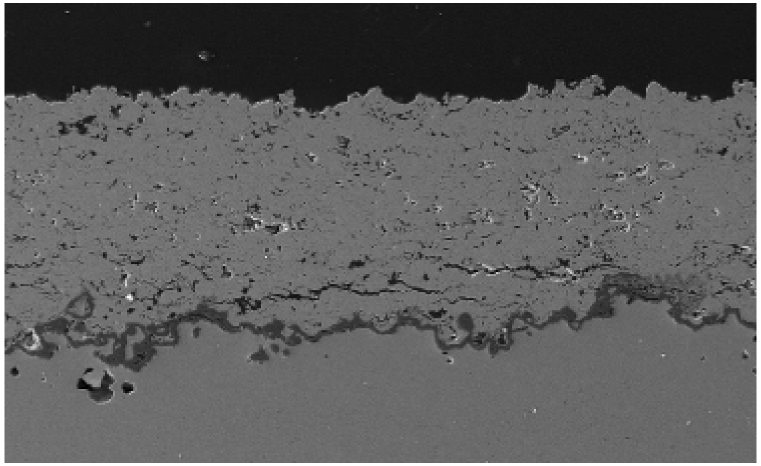

$(\alpha_0, \ldots)$ ⇨ $(\alpha, \ldots.) < (\alpha_0, \ldots.)$

http://dx.doi.org/10.21611/qirt.2012.399

Integrity assessment: cracks and delaminations

Heat Dirac pulse

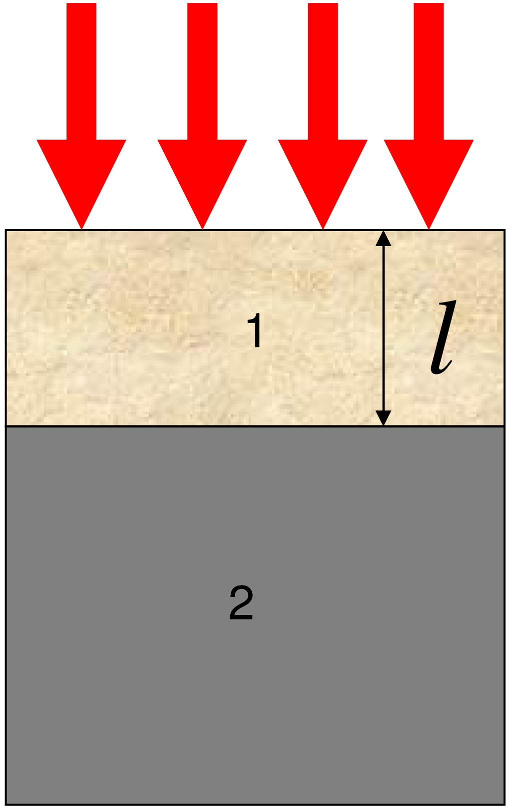

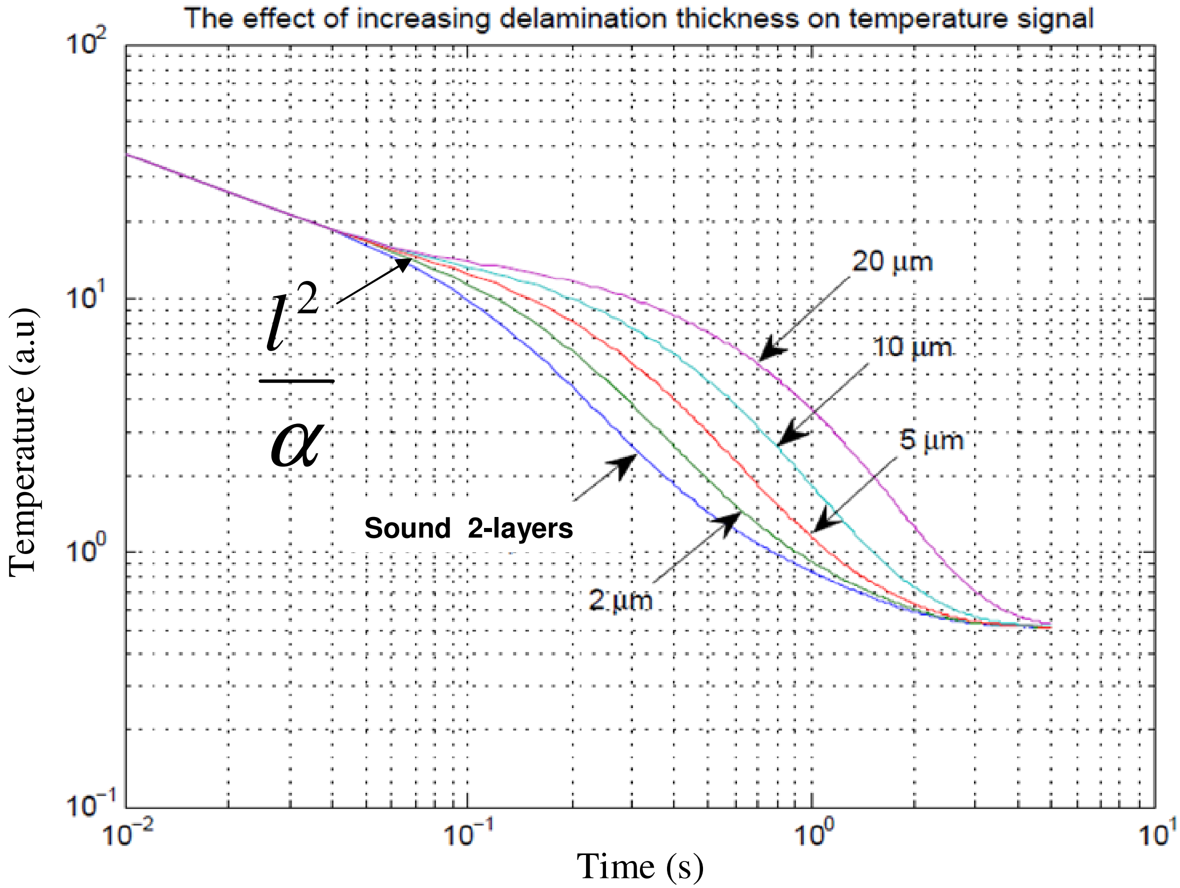

http://dx.doi.org/10.21611/qirt.2012.399

Crack growth ND detection on samples tested by cyclic oxidation

Superposition of two effects (sintering&cracking) with different relaxation times and magnitudes

⇩

No monotonic trend of thermal diffusivity vs. ageing time

⇩

Some information about cracking at the interface can be obtained from thermal diffusivity

http://dx.doi.org/10.21611/qirt.2012.399

Crack growth ND detection on samples tested for cyclic oxidation

28 disk shaped samples coated with a APS TBC

9 thin samples (T1) 254±10 µm

19 thick samples (T2) 328±9 µm

Porosity 15%

2 hours cycle: 1.5 hour dwell time@1050°C

Average lifetime was estimated on 2+2 samples (T1=1008±12 and T2=880±12 cycles)

Samples have been aged up a fixed percentages of the average lifetime. Thermal diffusivity of each sample was measured in the as sprayed condition and after different aging cycles.

http://dx.doi.org/10.21611/qirt.2012.399

Crack growth ND detection on thermally cycled samples – Thin TBC

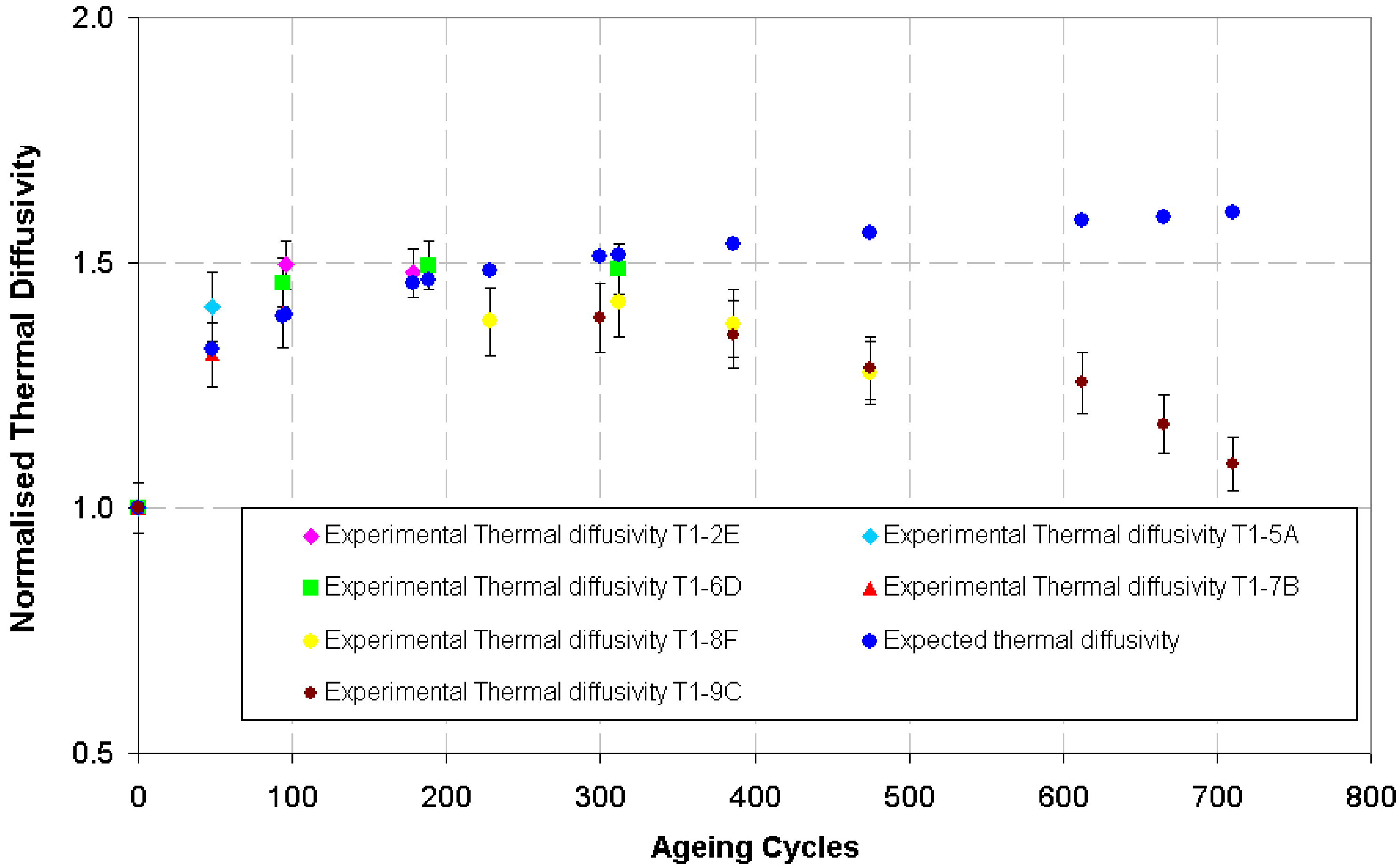

http://dx.doi.org/10.21611/qirt.2012.399

Crack growth ND detection on thermally cycled samples – Thick TBC

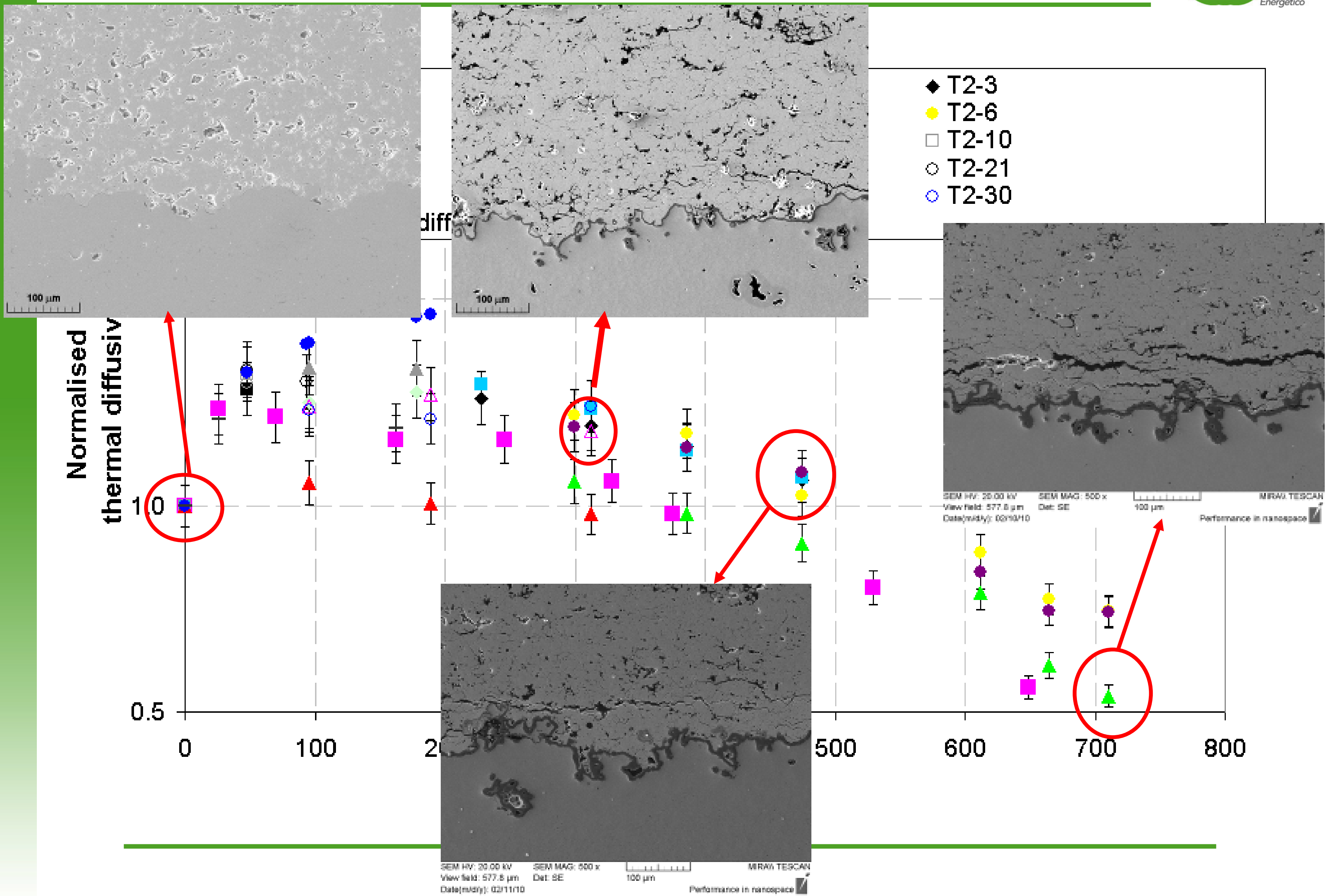

http://dx.doi.org/10.21611/qirt.2012.399

How to correlate the thermal diffusivity with the damage at the interface?

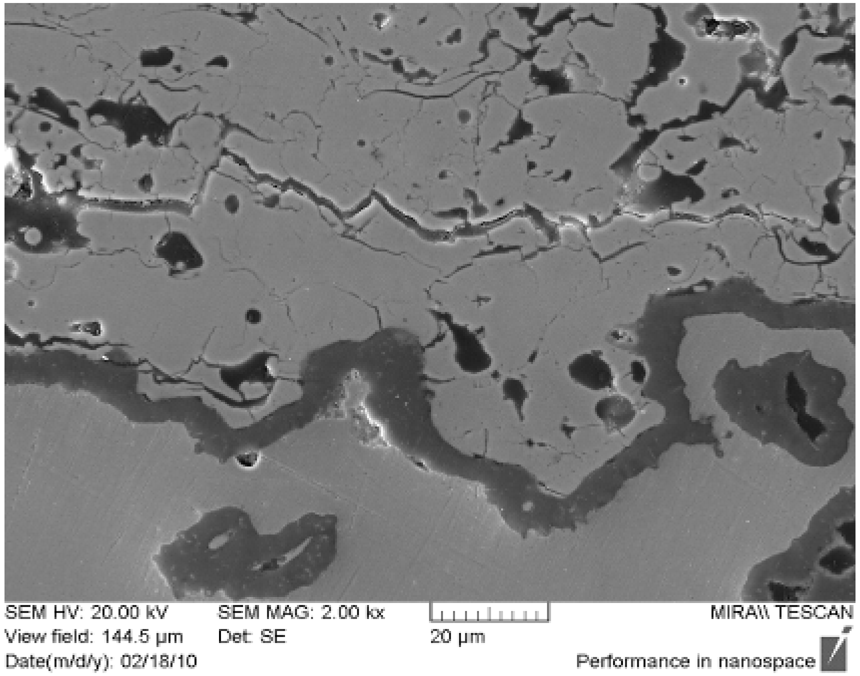

http://dx.doi.org/10.21611/qirt.2012.399

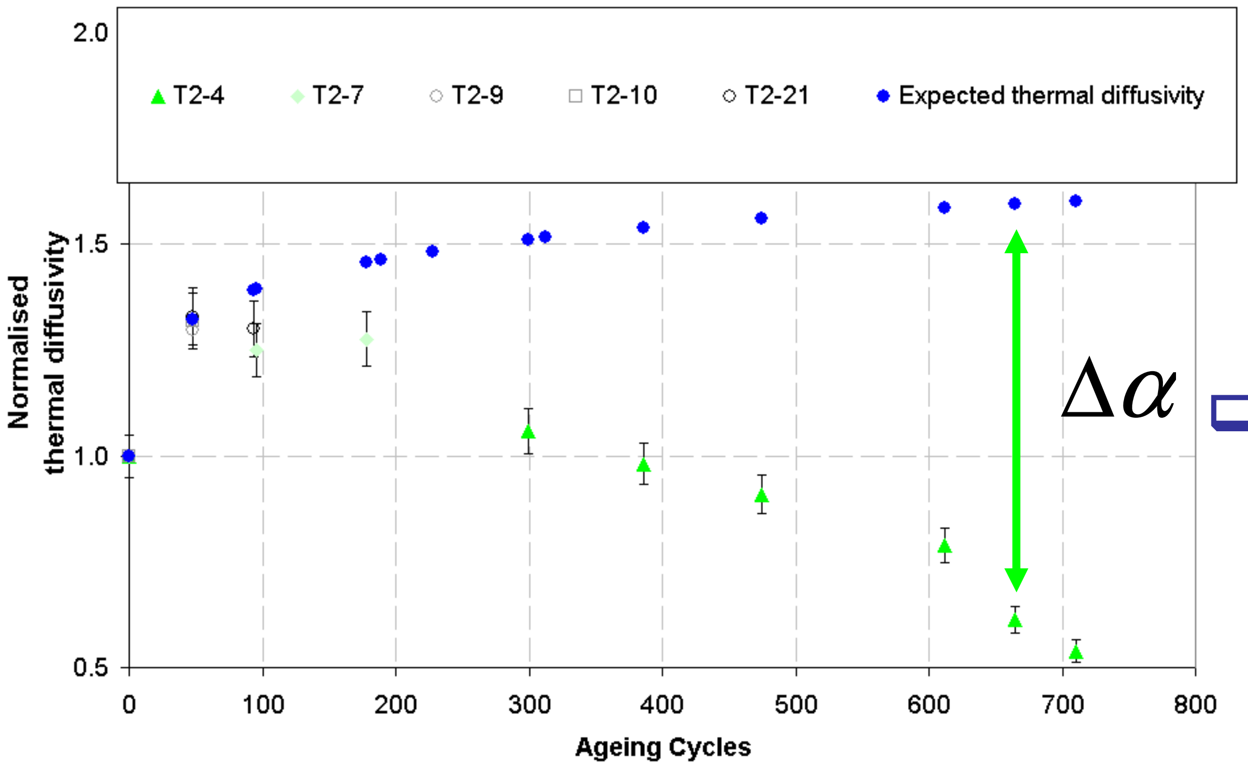

% of cracked interface

Modeling of the effect of cracks on TBC thermal diffusivity

http://dx.doi.org/10.21611/qirt.2012.399

Estimation of cracked interface by 2D- Inversion model

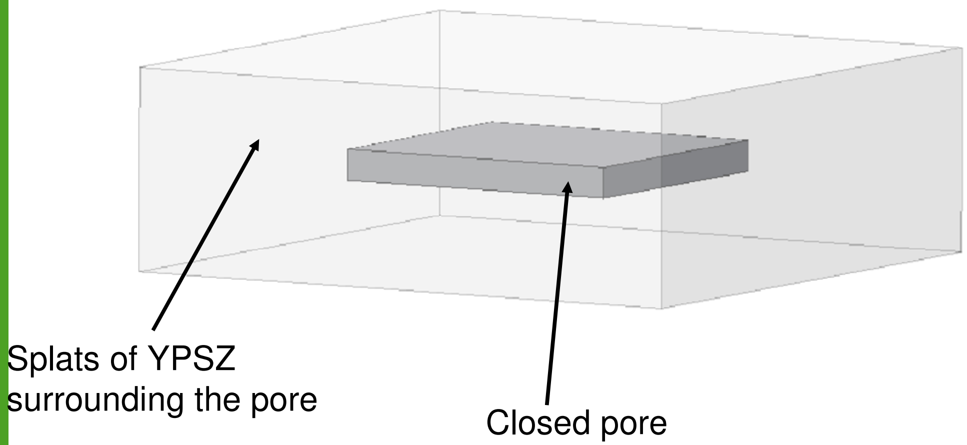

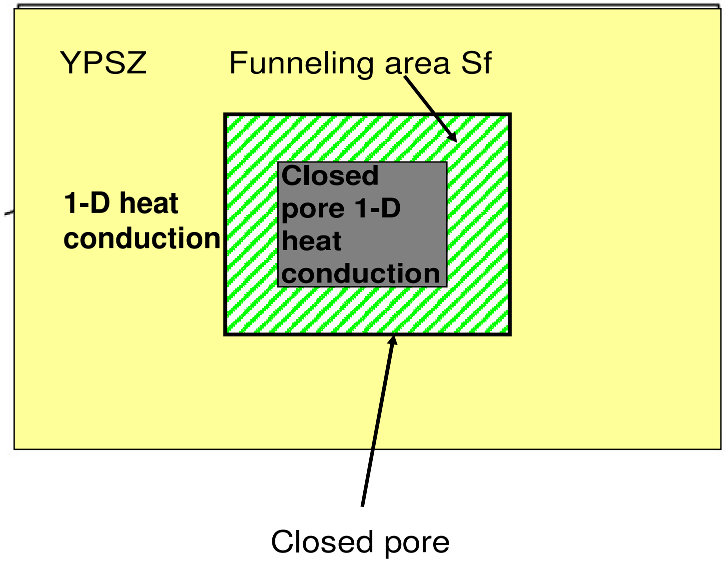

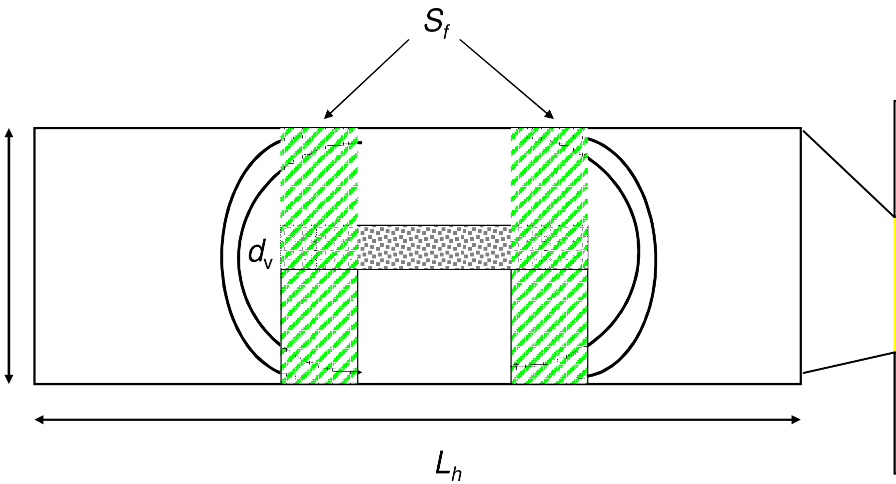

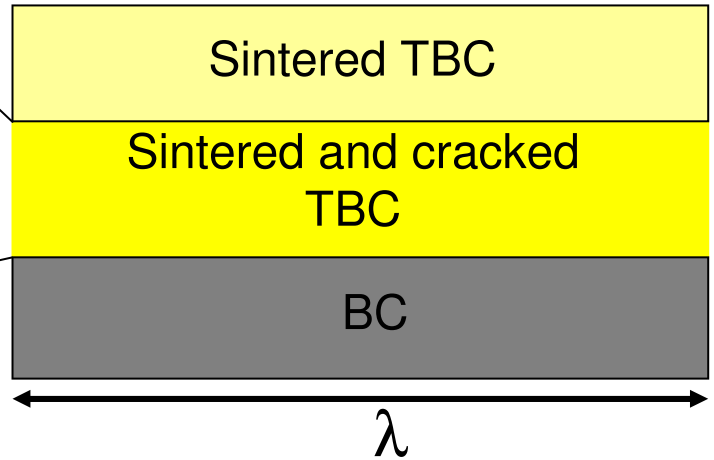

Golosnoy et al., Journal of Thermal Spray Technol. 14(2) 2005

http://dx.doi.org/10.21611/qirt.2012.399

How the cracked fraction of interface has been estimated from IA?

http://dx.doi.org/10.21611/qirt.2012.399

Estimation of cracked fraction of interface from IA

Cracks caused by thermal cycling have been supposed to be thicker and sharper than those originated during the spray process

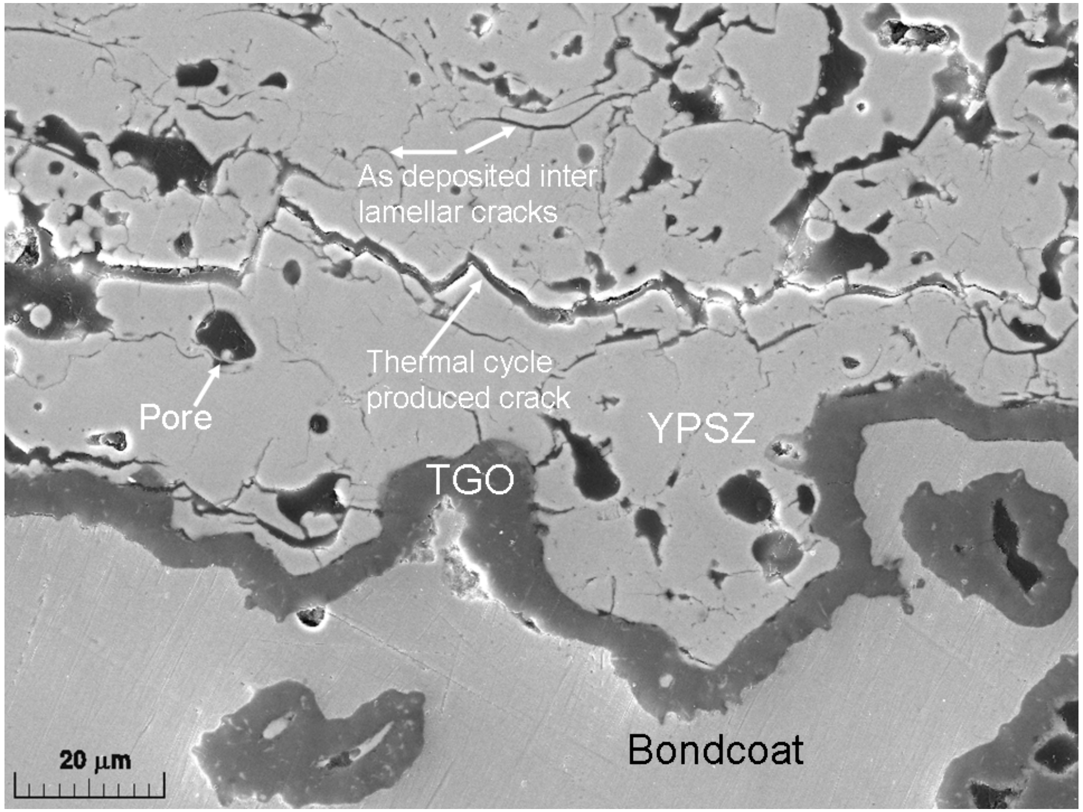

http://dx.doi.org/10.21611/qirt.2012.399

Estimation of cracked fraction of interface from IA

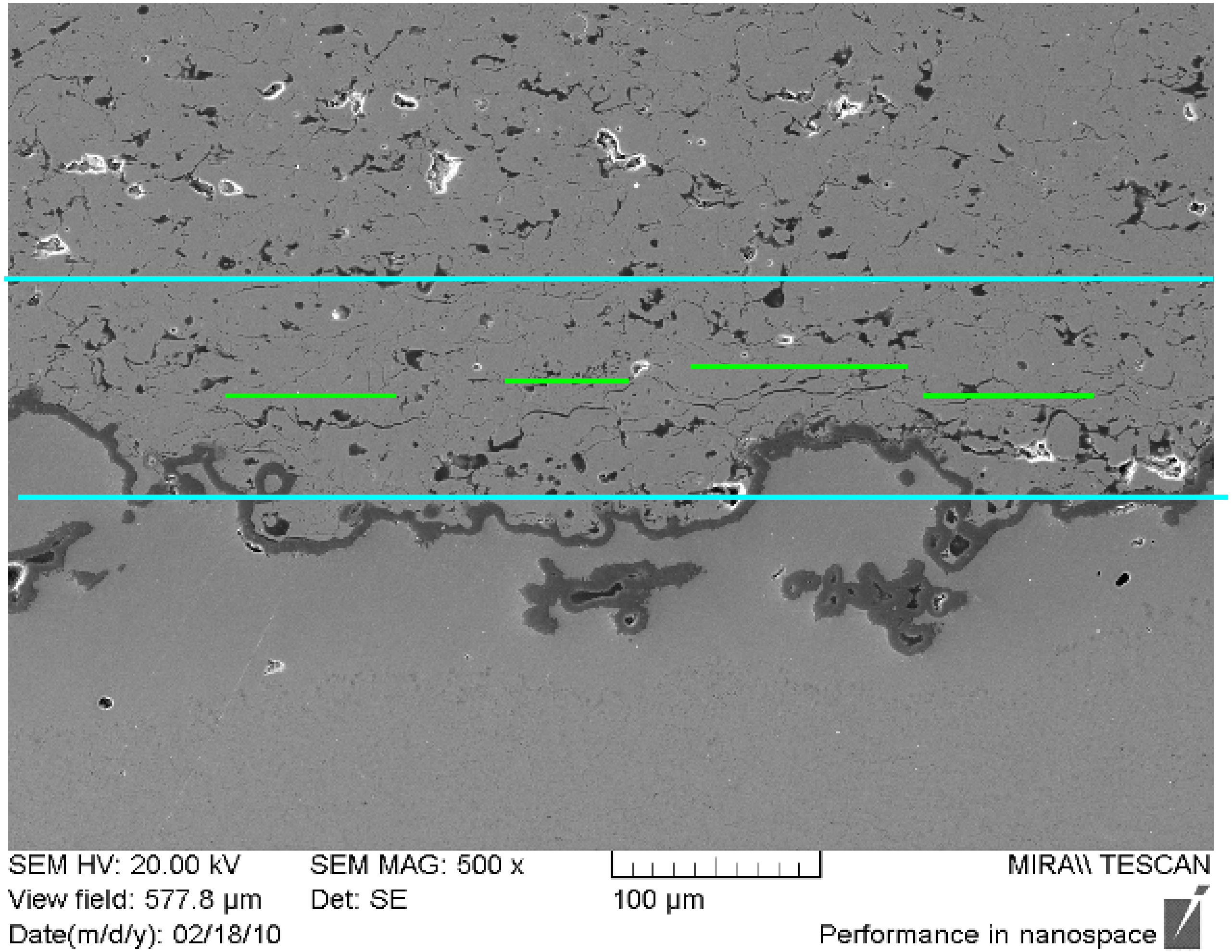

http://dx.doi.org/10.21611/qirt.2012.399

Estimation of cracked fraction of interface from IA

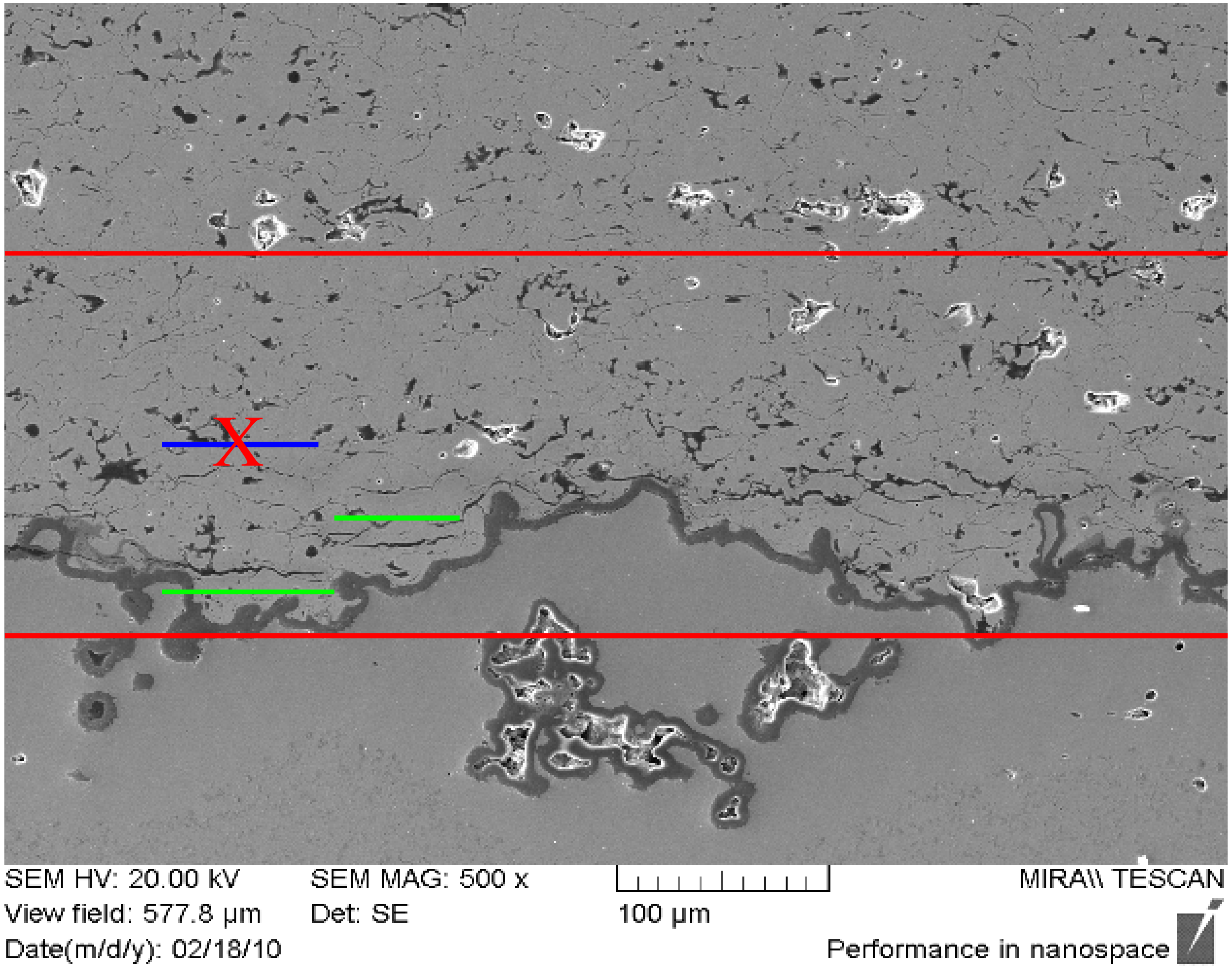

http://dx.doi.org/10.21611/qirt.2012.399

Estimation of cracked interface by 2D- Inversion model

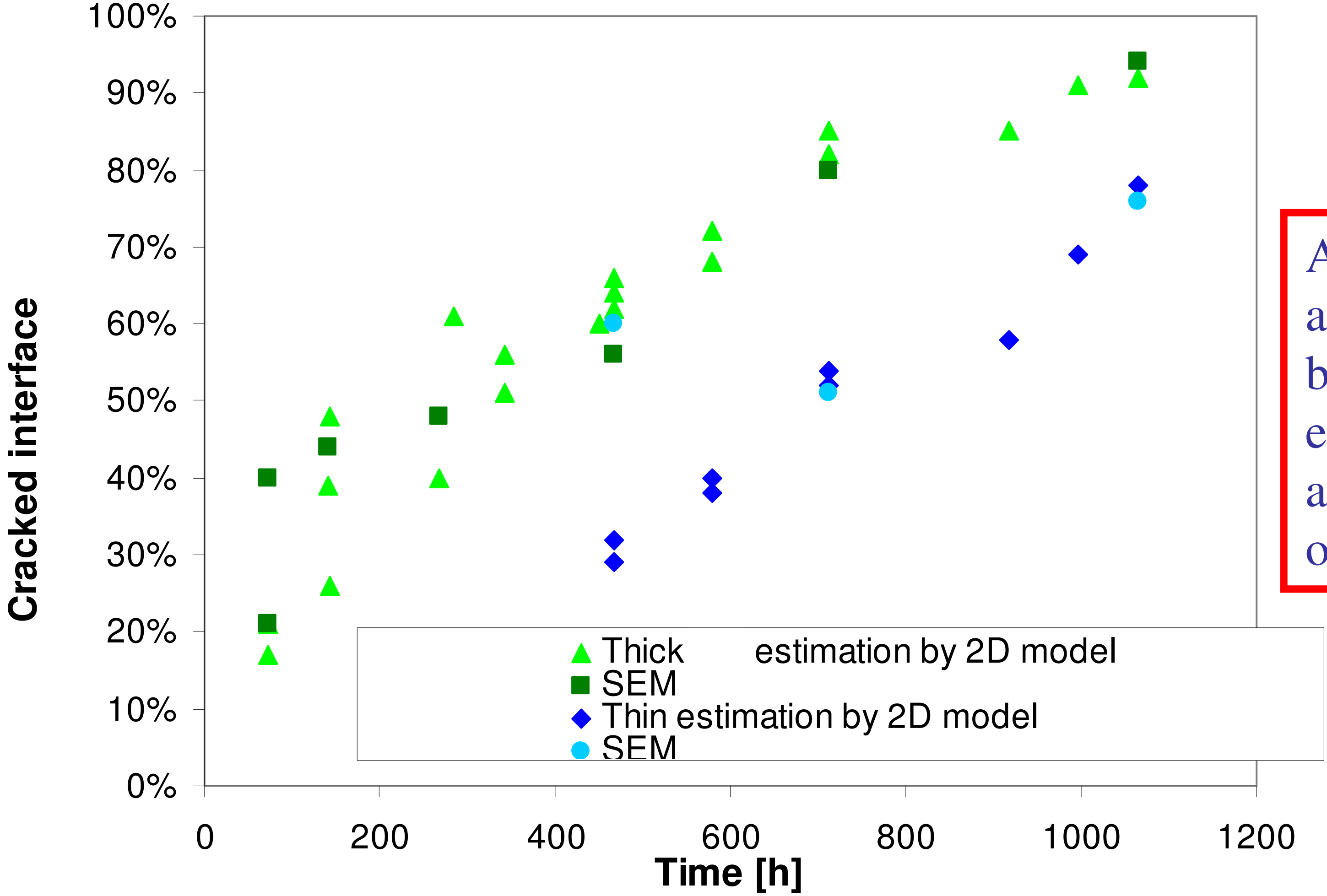

A good agreement between estimations and SEM is observed

http://dx.doi.org/10.21611/qirt.2012.399

Estimation of cracked interface by 2D- Inversion model

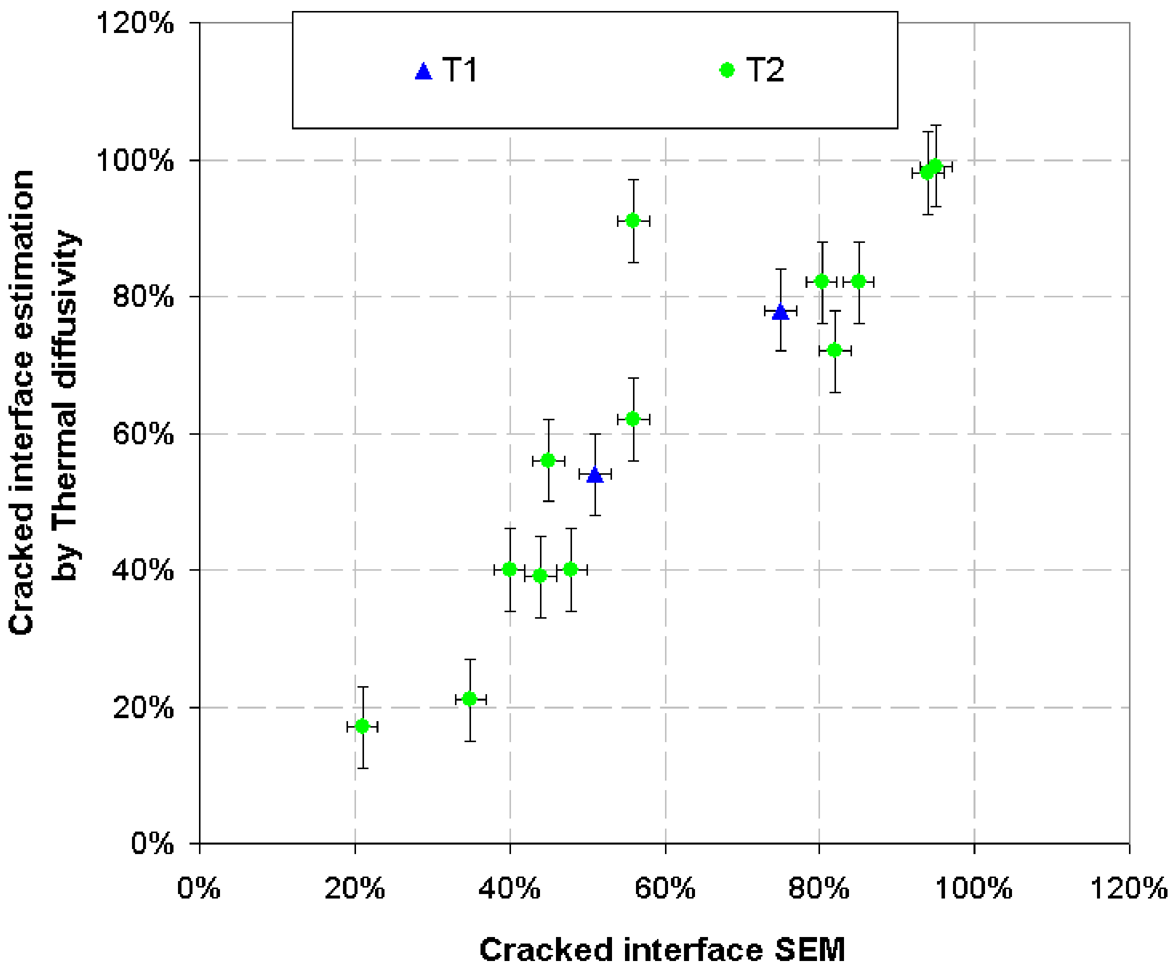

http://dx.doi.org/10.21611/qirt.2012.399

Estimation of cracked interface by 2D- Inversion model

- The crack thickness has been fixed equal to 3 µm for each sample at each ageing time. When necessary, to zeroing the inversion function, the thickness has been increased up to values of 6 - 11 µm for ageing times close to the end of TBC life.
- For data referring to roughly 50% of TBC life, a crack thickness value intermediate between 3 µm and the maximum value was adopted.

http://dx.doi.org/10.21611/qirt.2012.399

How to avoid the "tuning" effect of the crack thickness in the inversion model?

http://dx.doi.org/10.21611/qirt.2012.399

A figure of merit

Consider the trend of cracked fraction vs. crack thickness and to look for a simple fitting function whose free parameters can be related to the damage at the interface

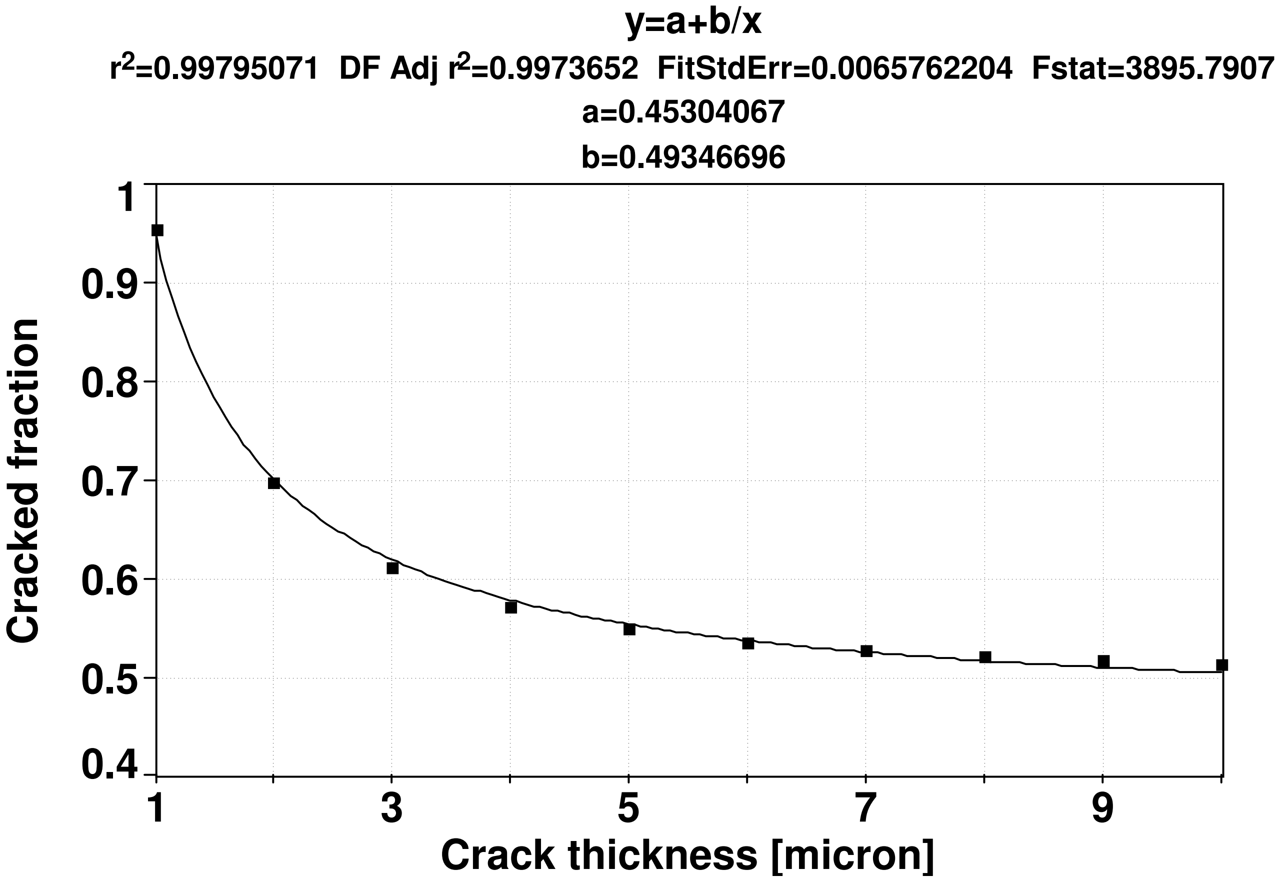

F. Cernuschi, S. Capelli, P. Bison, S. Marinetti, L. Lorenzoni, E. Campagnoli and C. Giolli, Acta Materialia 59 (2011) 6351–6361

http://dx.doi.org/10.21611/qirt.2012.399

A figure of merit

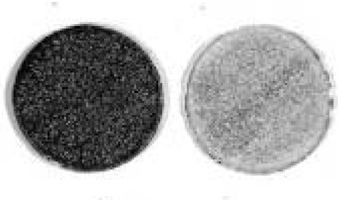

8.0±0.9 10^{-4}

872 cycles

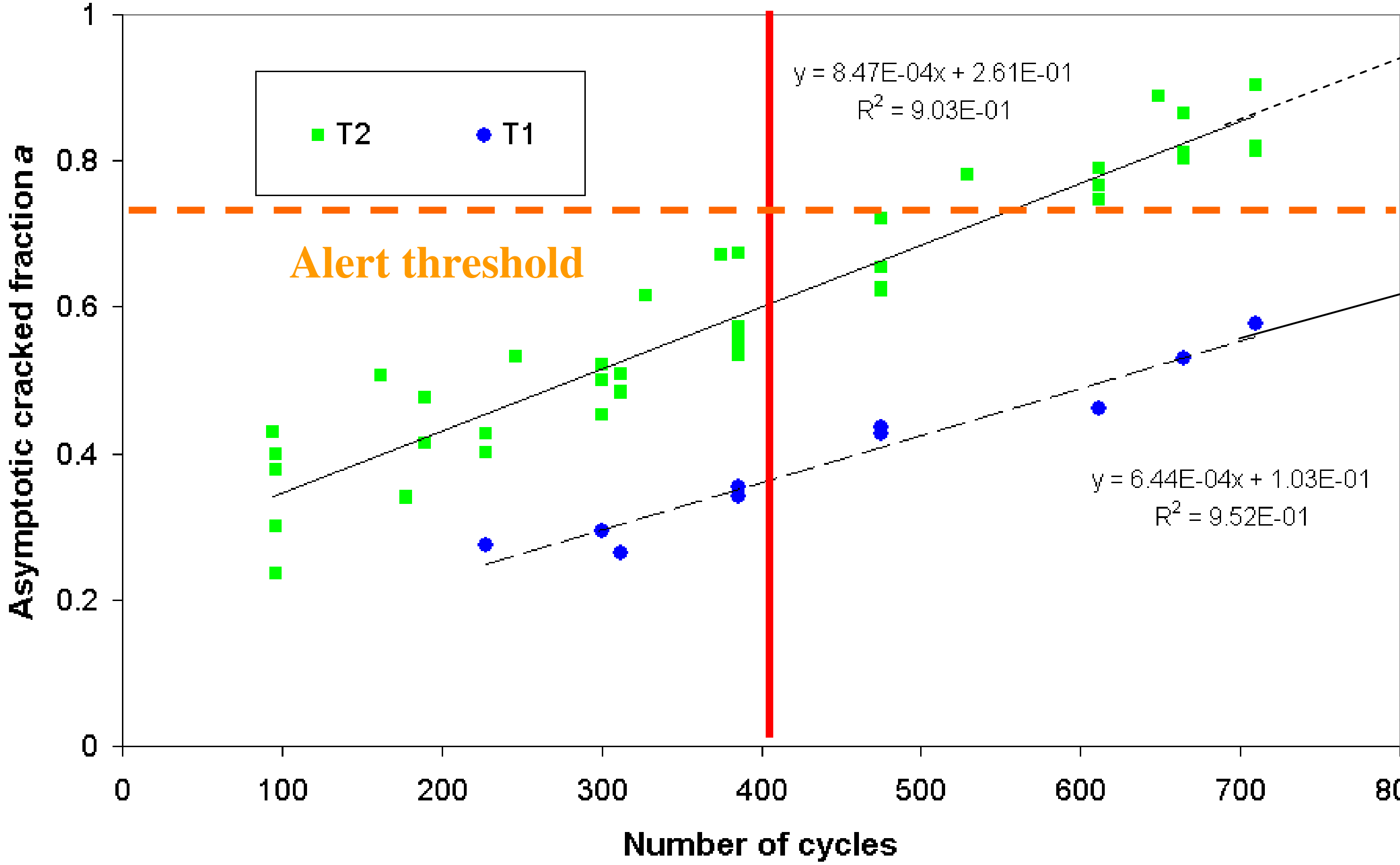

1392 cycles

http://dx.doi.org/10.21611/qirt.2012.399

Conclusions

- A 2D model has been used for better estimating the cracked fraction of the interface between APS TBC and BC, especially at early stage when there are several short cracks.
- A figure of merit incorporating both cracked fraction and crack thickness was also proposed for ranking the damage and obtaining indications on the failure time

http://dx.doi.org/10.21611/qirt.2012.399

Microstructural characterisation of APS TBC by thermal diffusivity evaluation and sintering forecasts

F. Cernuschi, I.G. Golosnoy, P. Bison, A. Moscatelli, R. Vassen, H-P Bossmann and S. Capelli, "Microstructural Characterization of Porous Thermal Barrier Coatings by IR gas porosimetry and sintering forecasts'' submitted to Acta Materialia

http://dx.doi.org/10.21611/qirt.2012.399

The idea

As sprayed TBC

IA SEM

Thermal diffusivity in gases

MIP

Microstructural parameters of as sprayed TBC

Sintering modeling

Forecast evolution of microstructural parameters with sintering & TD

Thermal diffusivity modeling

Comparison with experimental IA, MIP and TD on sintered TBC

http://dx.doi.org/10.21611/qirt.2012.399

Thermal diffusivity in different gases

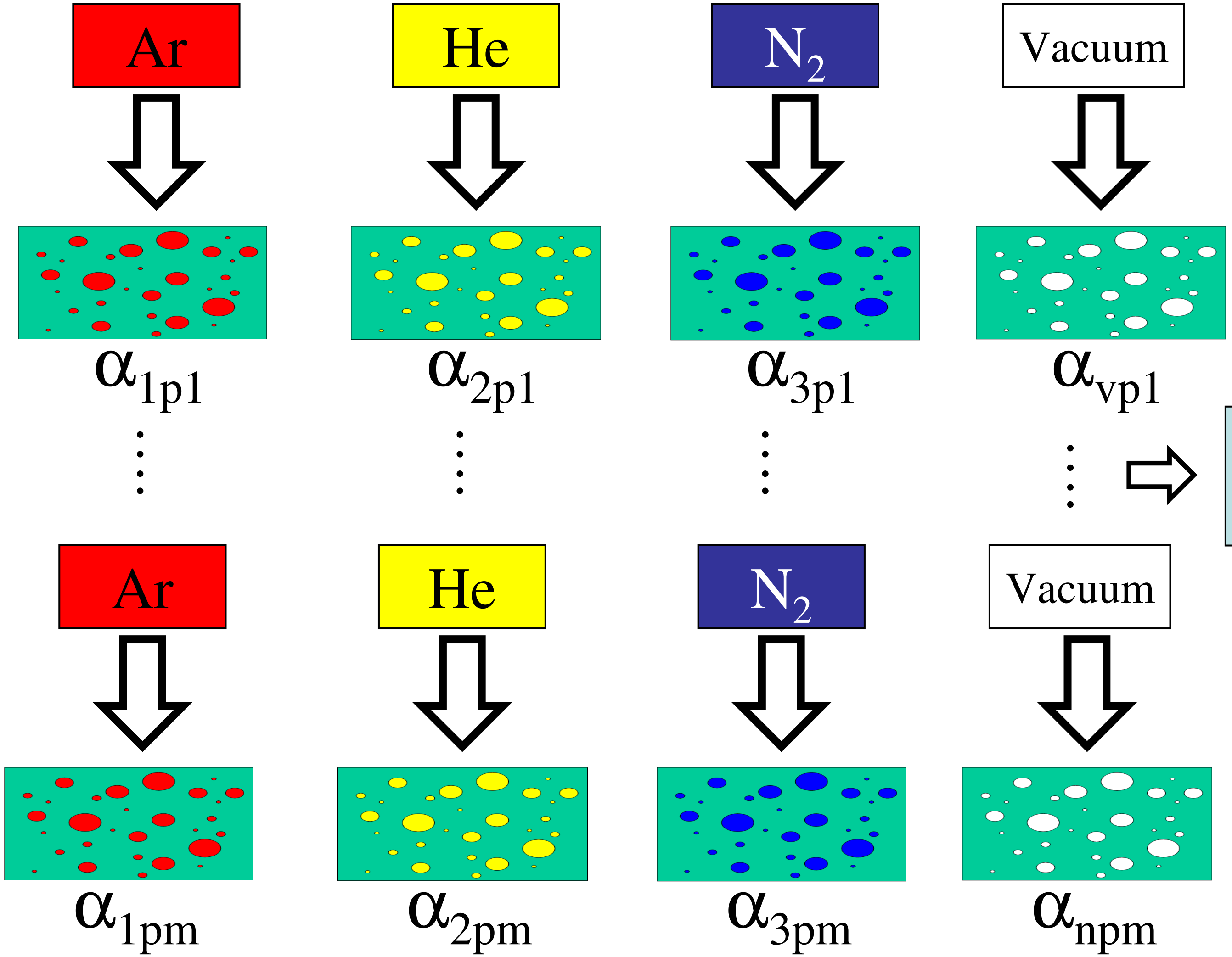

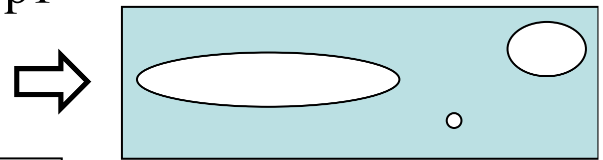

Effective crack opening

Aspect ratio of inter lamellar pores

F. Cernuschi, P. Bison, A. Moscatelli, *Acta Materialia*., 57 (2009) 3460–3471

http://dx.doi.org/10.21611/qirt.2012.399

Modelling of porous solids

Symmetric models

Asymmetric models

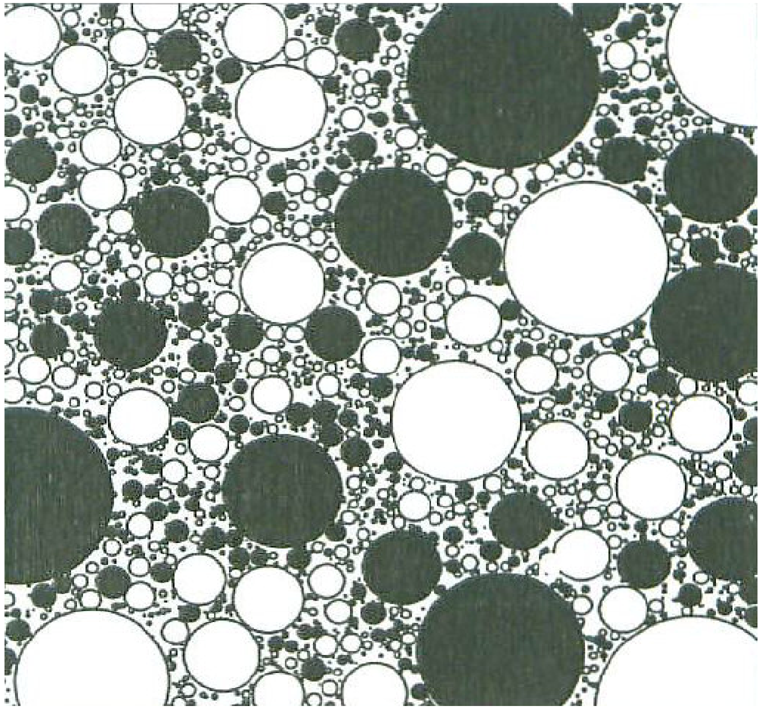

TBC

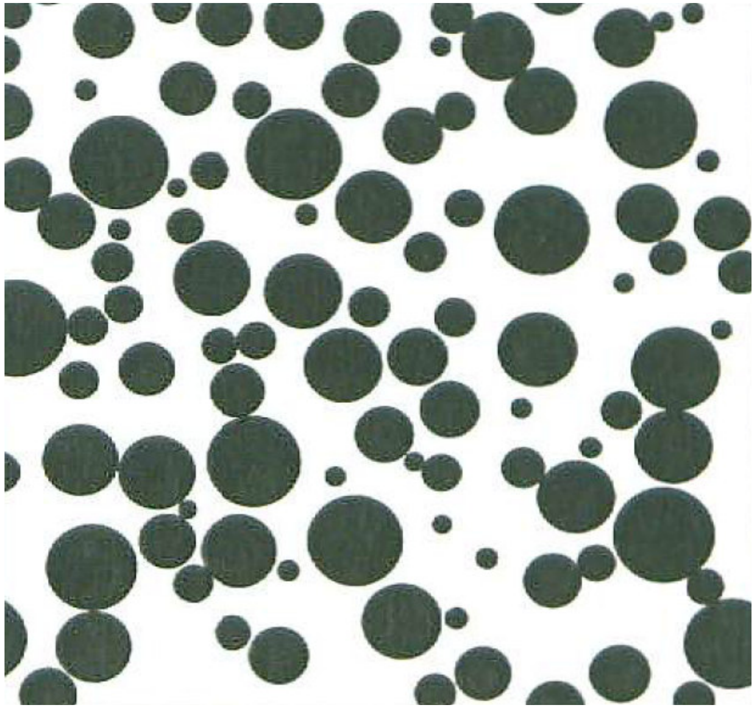

⇩

Asymmetric model

http://dx.doi.org/10.21611/qirt.2012.399

Modelling of porous solids

$$\frac{k}{k_m} = (1 - f)^X$$

$$X = \frac{1 - \cos^2\alpha}{1 - F} + \frac{\cos^2\alpha}{2F}$$

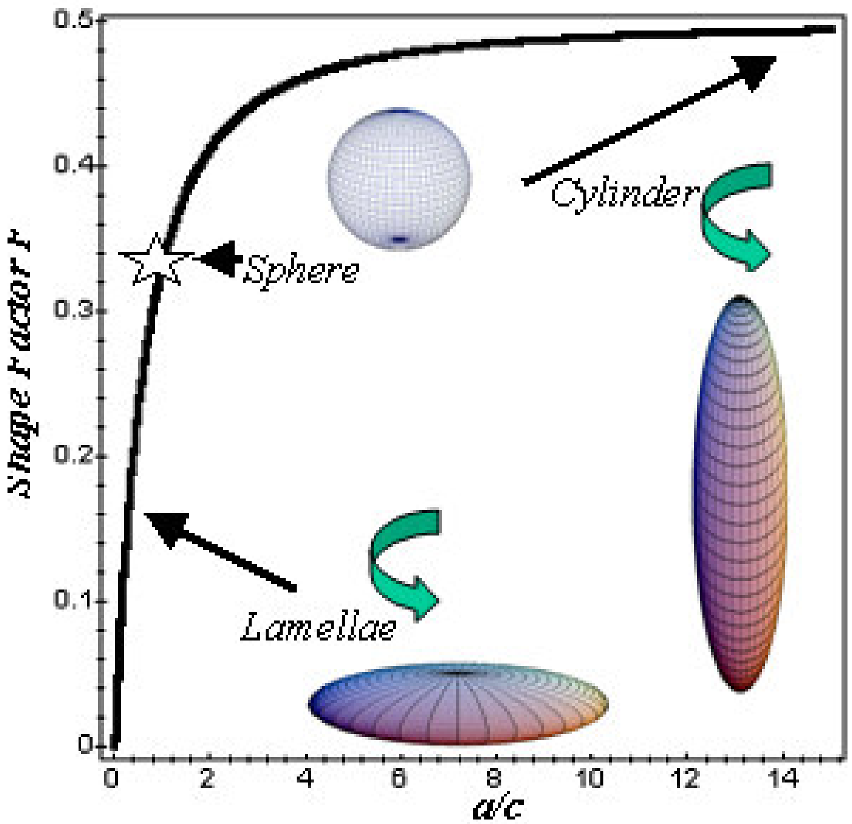

D.A.M Bruggeman, Annalen der Physik n°5 [24] 1935

http://dx.doi.org/10.21611/qirt.2012.399

Modelling of porous solids

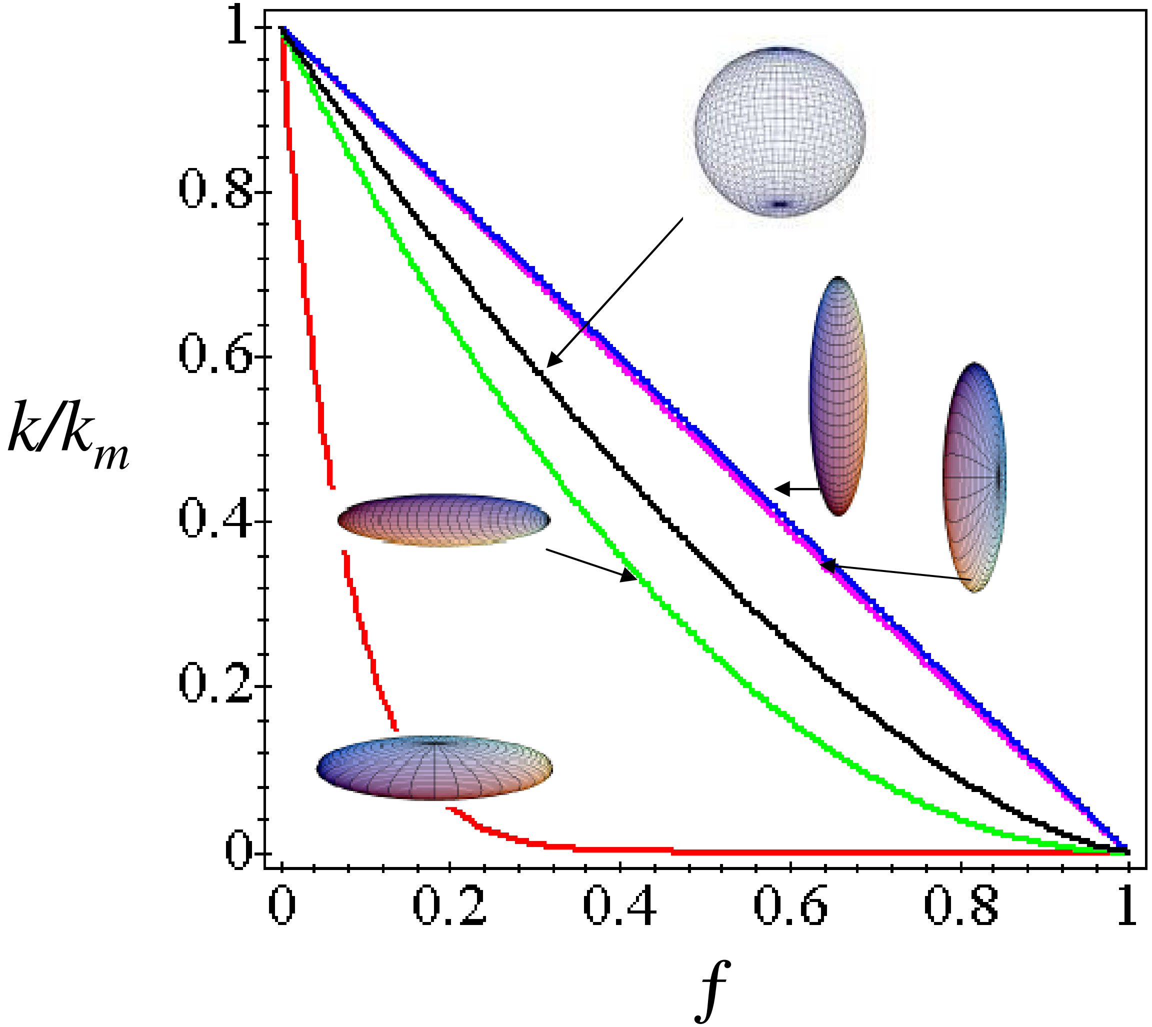

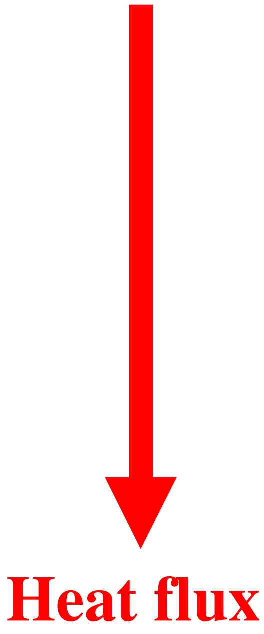

http://dx.doi.org/10.21611/qirt.2012.399

Modelling of porous solids - thermal conductivity of gases within pores

k_{bulk} H_2 Ar N_2

$\neq$

k_{pores}

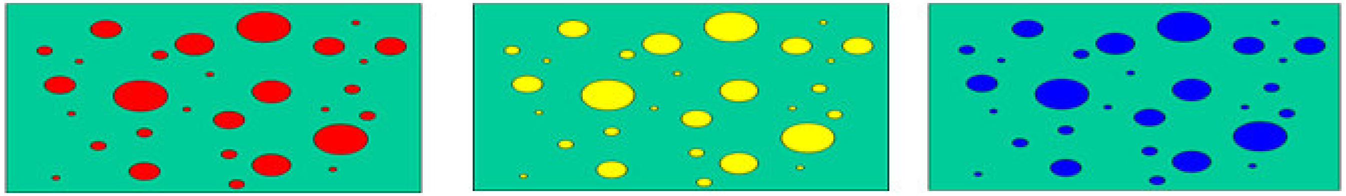

http://dx.doi.org/10.21611/qirt.2012.399

Modelling of porous solids - thermal conductivity of gases within pores

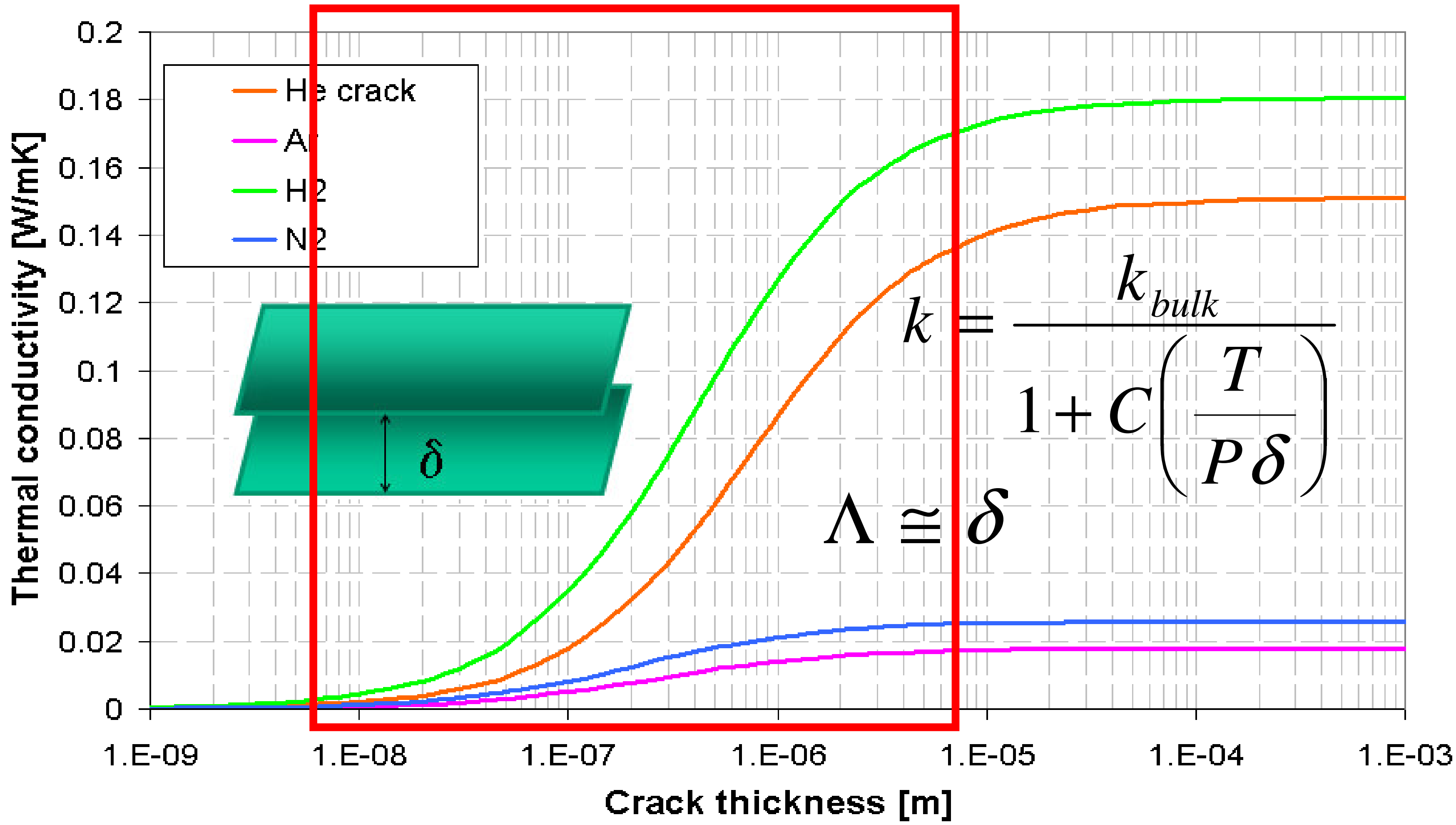

http://dx.doi.org/10.21611/qirt.2012.399

Modelling of porous solids - thermal conductivity of gases within pores

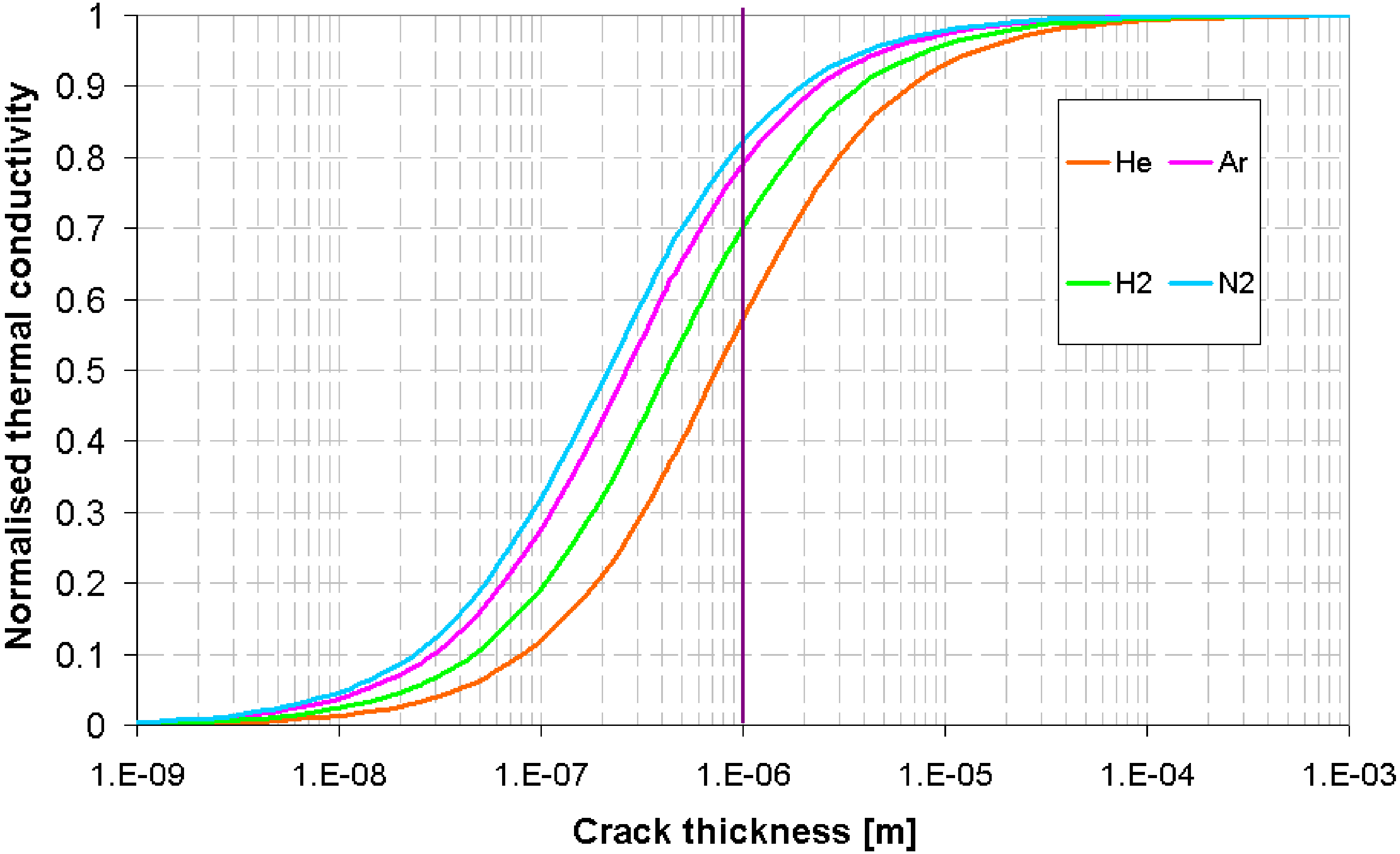

http://dx.doi.org/10.21611/qirt.2012.399

Modelling of porous solids - thermal conductivity of gases within pores

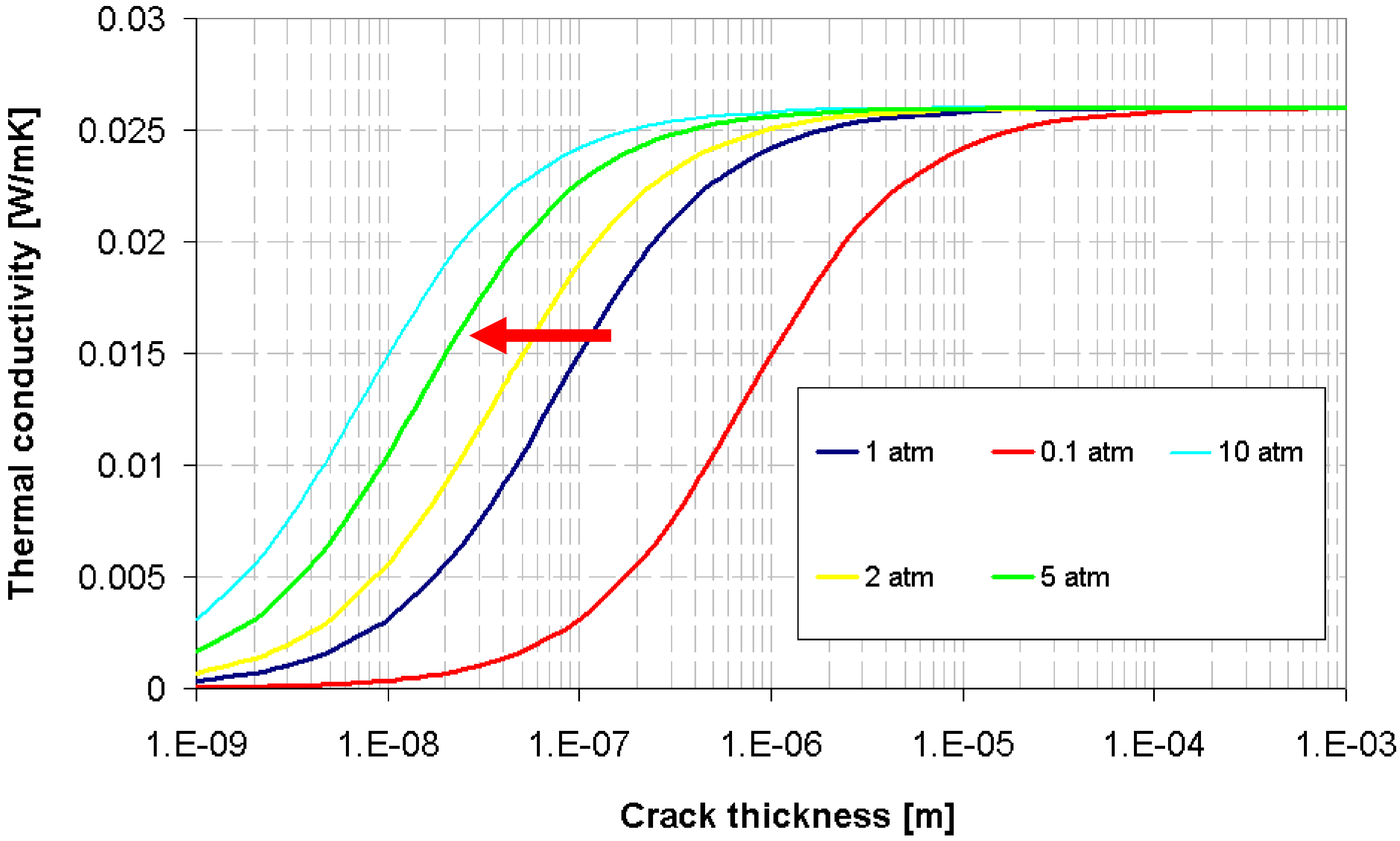

http://dx.doi.org/10.21611/qirt.2012.399

Modelling of porous solids

How is it possible to simultaneously model several types of pores?

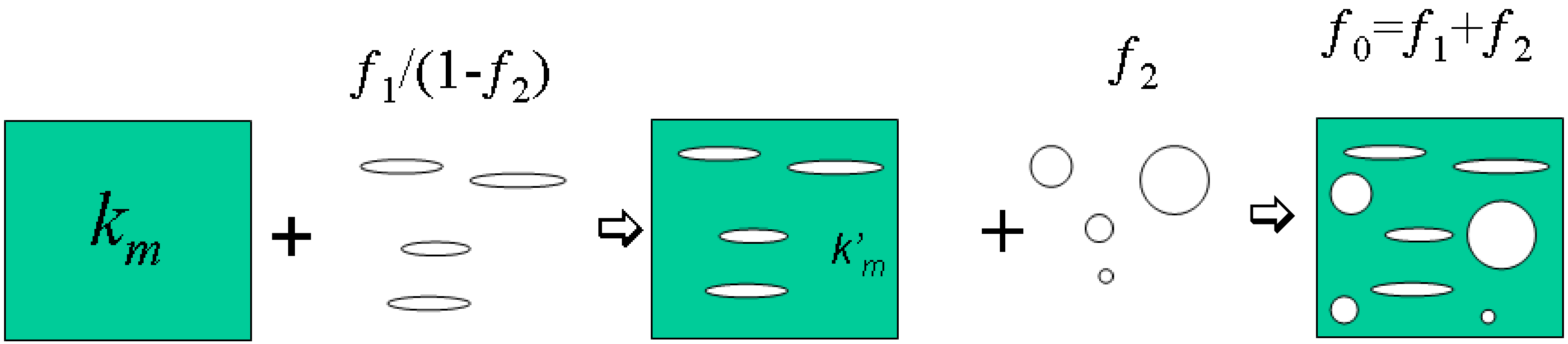

$$k = \frac{1}{2}\left\{\Phi\left(\Psi\left(k_m, \frac{f_1}{(1-f_2)}\right), f_2\right) + \Psi\left(\Phi\left(k_m, \frac{f_2}{(1-f_1)}\right), f_1\right)\right\}$$

http://dx.doi.org/10.21611/qirt.2012.399

The samples - YPSZ APS TBC

Sample Code	Thickness [µm]	Shape	Size [mm]	Heat treated	Characterised by
WD1	427±16	disk	9.81	Y	Thermal diffusivity and SEM
WD2	416±15	disk	9.81	Y	Thermal diffusivity and SEM
WD3	400±21	disk	9.81	Y	Thermal diffusivity and SEM
WD4	414±13	Square	20	N	SEM
WD6	n.a.	Rectangular	10 X40	N	Hg intrusion Porosimetry
WD7	n.a.	Rectangular	10 X40	N	Hg intrusion Porosimetry
WD8	n.a.	Rectangular	10 X40	Y	Hg intrusion Porosimetry
WD9	n.a.	Rectangular	10 X40	Y	Hg intrusion Porosimetry

As sprayed

Heat treated 200 h @1250°C

http://dx.doi.org/10.21611/qirt.2012.399

The samples - YPSZ APS TBC

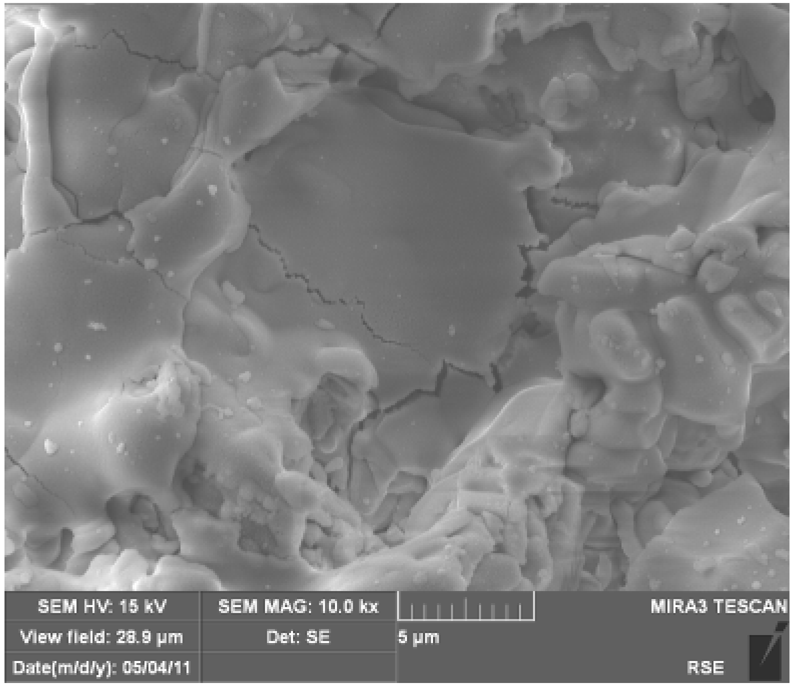

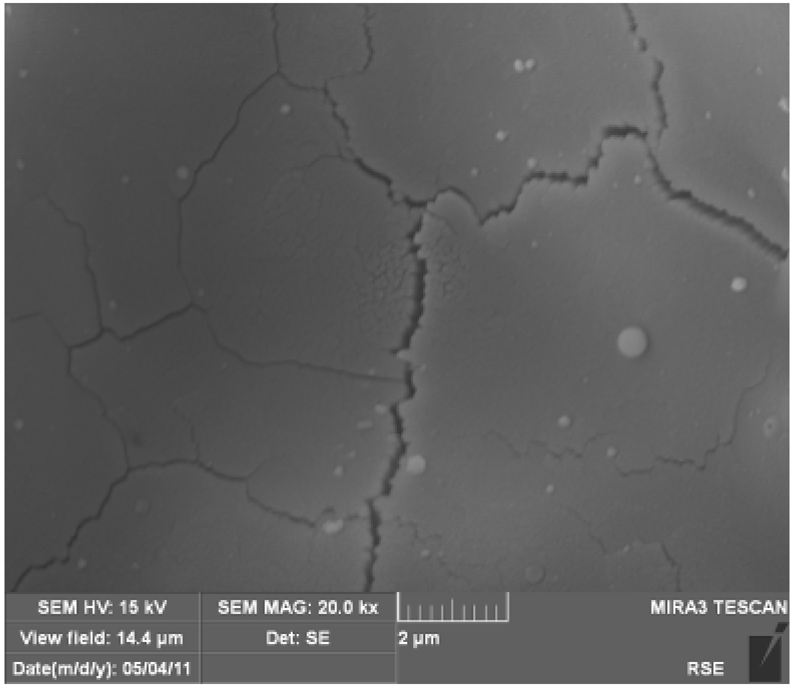

Vertical intra-lamellar cracks

http://dx.doi.org/10.21611/qirt.2012.399

The samples - YPSZ APS TBC

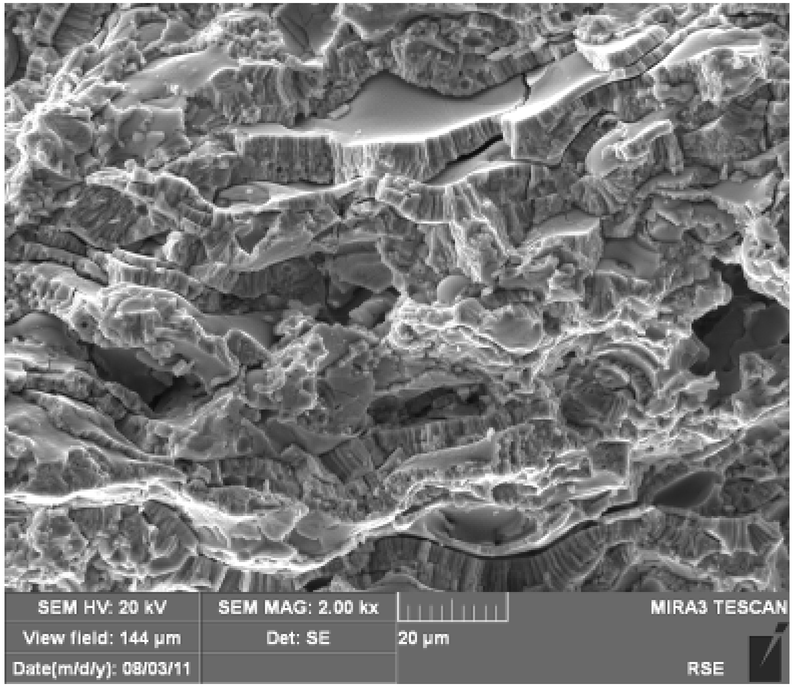

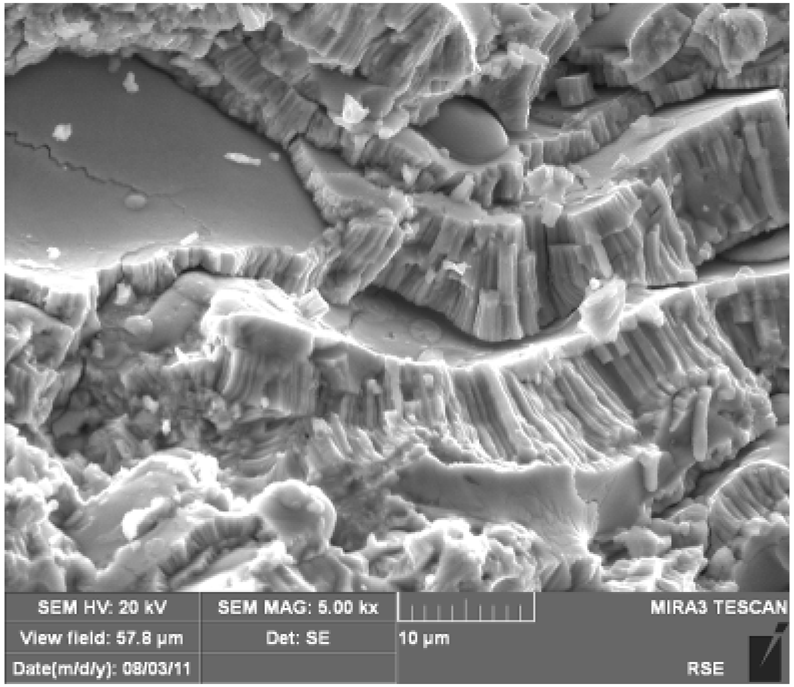

Horizontal inter-lamellar pores

Vertical intra-lamellar cracks

Globular pores

http://dx.doi.org/10.21611/qirt.2012.399

IA characterisation

Elongation (e>3) and orientation criteria

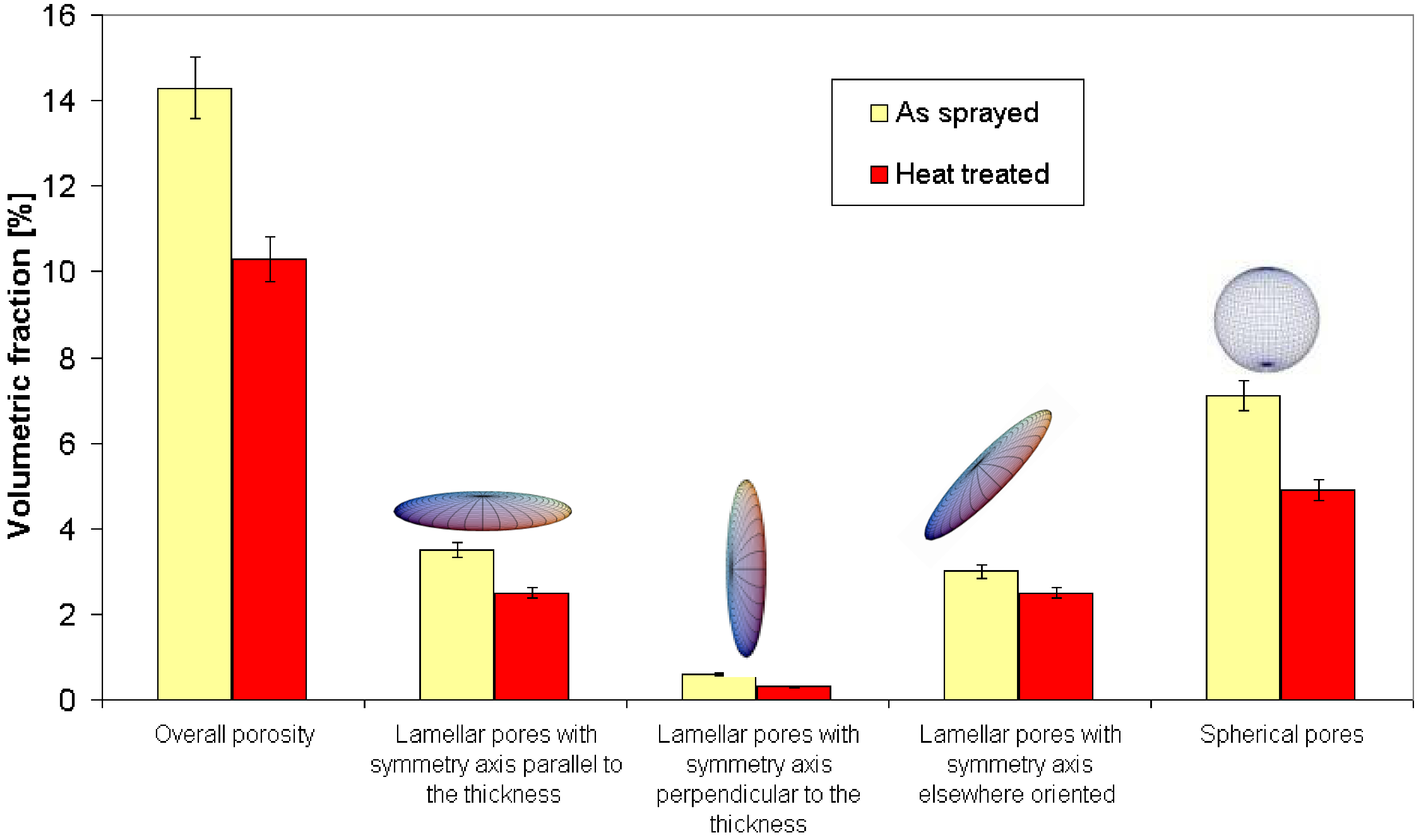

http://dx.doi.org/10.21611/qirt.2012.399

Experimental thermal diffusivity data

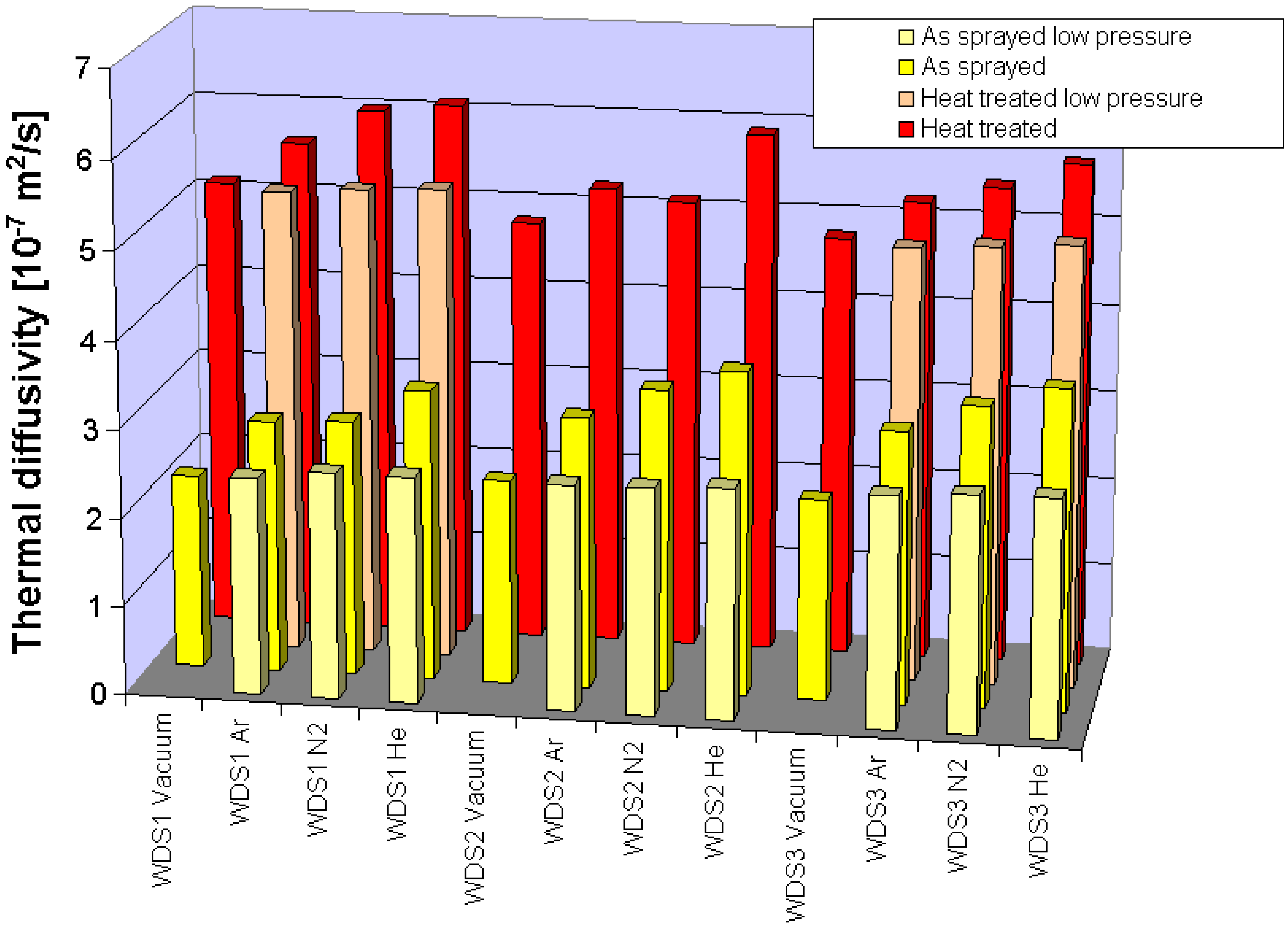

http://dx.doi.org/10.21611/qirt.2012.399

Experimental thermal diffusivity data

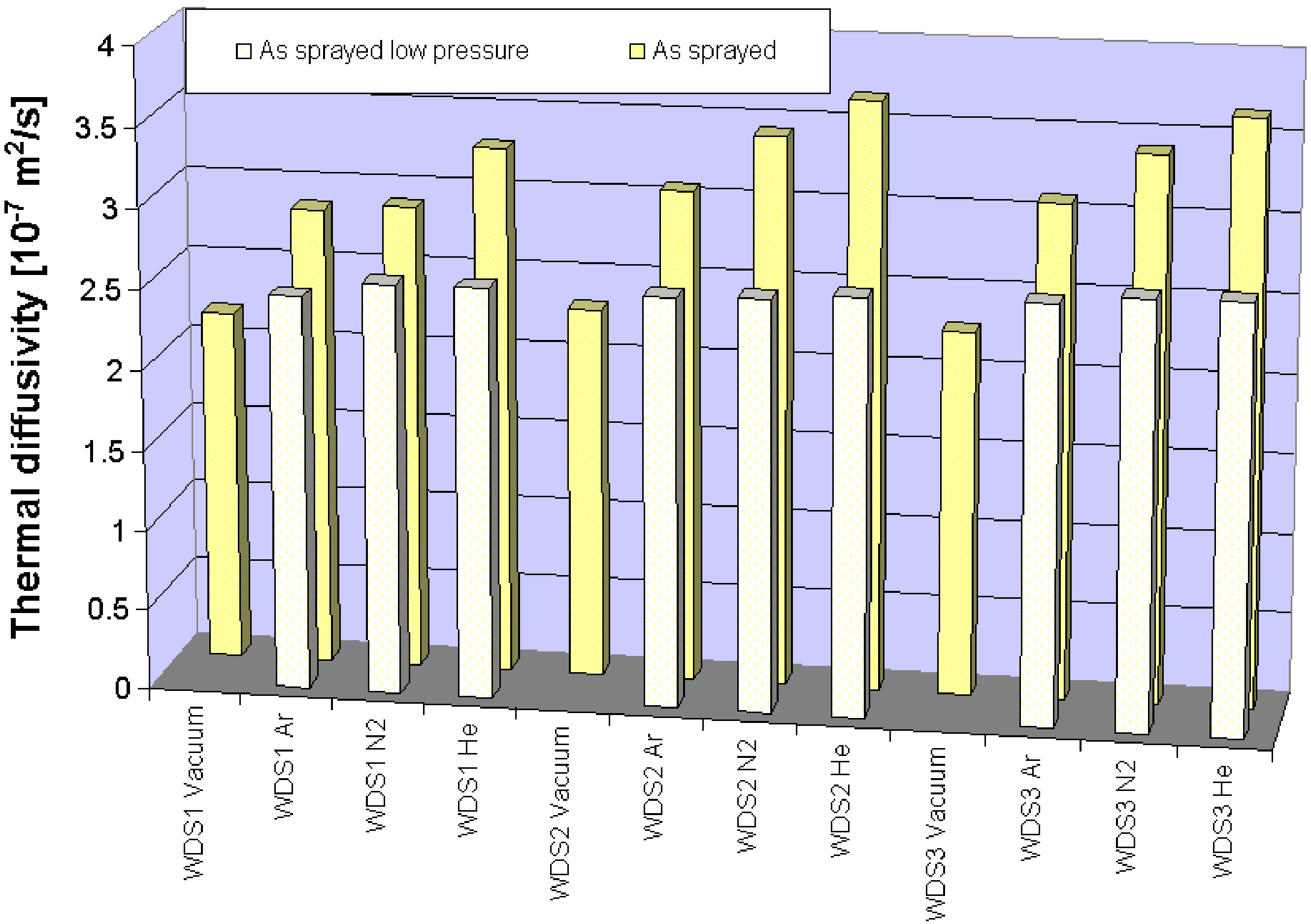

http://dx.doi.org/10.21611/qirt.2012.399

Input of the inversion code

As lamellar porosity parallel oriented to the heat flux **plays the major role in reducing** the thermal diffusivity, starting from the IA volumetric fractions, in the inversion code, porosity has been divided into two classes: parallel inter-lamellar pores and spheres.

Inter-lamellar parallel=true inter-lamellar parallel+1/3 elsewhere oriented lamellar

4.1% **1%**

Spheres=True spheres+2/3 elsewhere oriented lamellar+ vertical intra-lamellar cracks.

6.15% **2%** **0.55%**

5.1%+8.7%=13.8%

7 equations for each sample (vacuum , three gases, two pressures)

Average crack thickness and aspect ratio

http://dx.doi.org/10.21611/qirt.2012.399

Output of the inversion code

Porosity 13.8

WDS1 as Sprayed

a/c=1/38

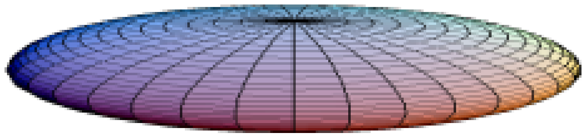

0.088±0.005 μm

Porosity 13.1

Specific surface area: $1.82 \cdot 10^6$ m^2/m^3

WDS2 as Sprayed

a/c=1/37

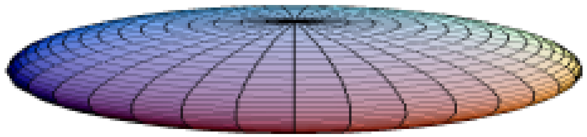

0.163±0.008 μm

Specific surface area: $1.0 \cdot 10^6$ m^2/m^3

WDS3 as Sprayed

a/c=1/37

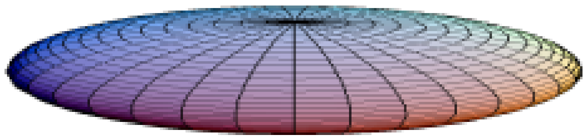

0.163±0.008 μm

Specific surface area: $1.0 \cdot 10^6$ m^2/m^3

Porosity 14.4

http://dx.doi.org/10.21611/qirt.2012.399

Input for the sintering code

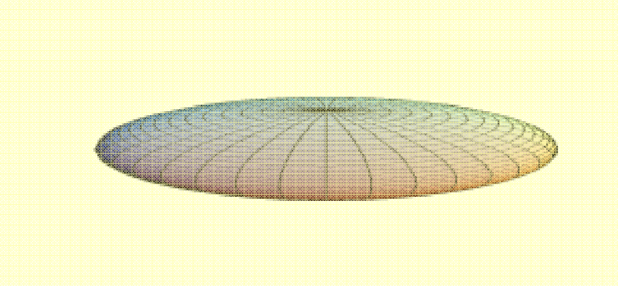

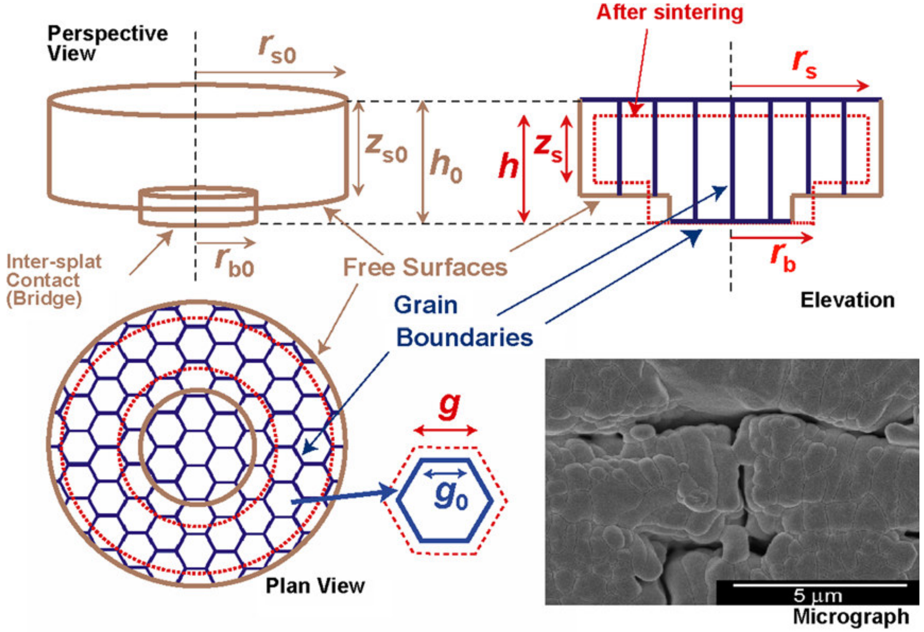

Bruggeman Model → Cipitria Model

Translation

Cipitria A., Golosnoy I.O., Clyne T.W., Acta Mater. 57, (2009), 980 – 992.

http://dx.doi.org/10.21611/qirt.2012.399

The Cipitria's sintering code

Surface and grain boundary diffusion, together with grain boundary migration

Grain boundary diffusion, leading to through-thickness shrinkage (reduction in r_s, h),

Surface diffusion contributes to pore spheroidization, i.e. reduces zs, causing the half-height of the pore $(h\text{-}z_s)$ to increase, and increases r_b.

Grain boundary migration causes an increase in lateral (in-plane) grain size, g, and hence a reduction in Ns

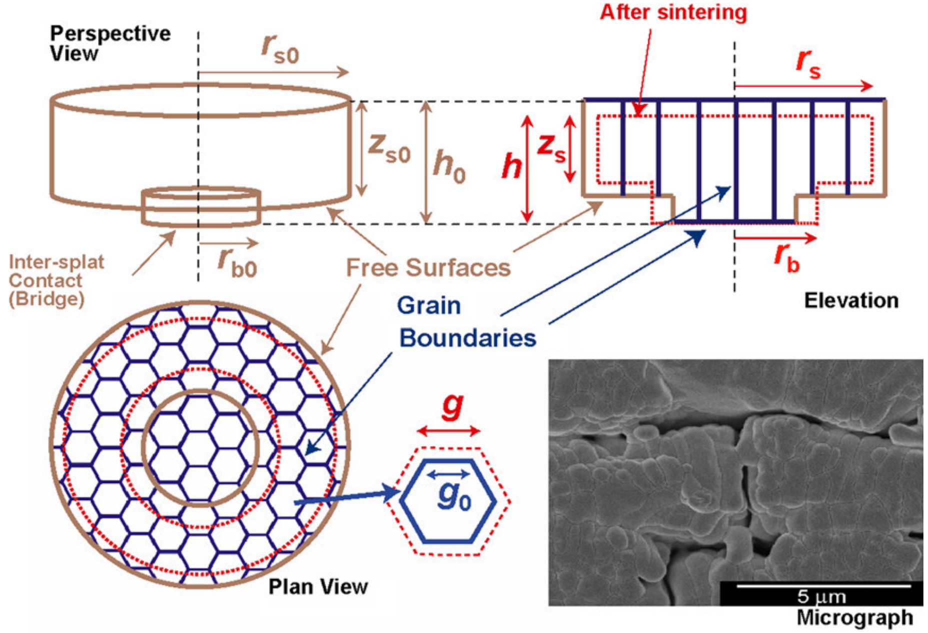

http://dx.doi.org/10.21611/qirt.2012.399

The Cipitria's sintering code

Grain boundary diffusion
(reduction in a and induced increase in x_b)

Surface diffusion
spheroidization of microcracks, i.e. reduces y_c, which promotes opening of the microcracks ($(a-y_c)$ increases), and increases x_b.

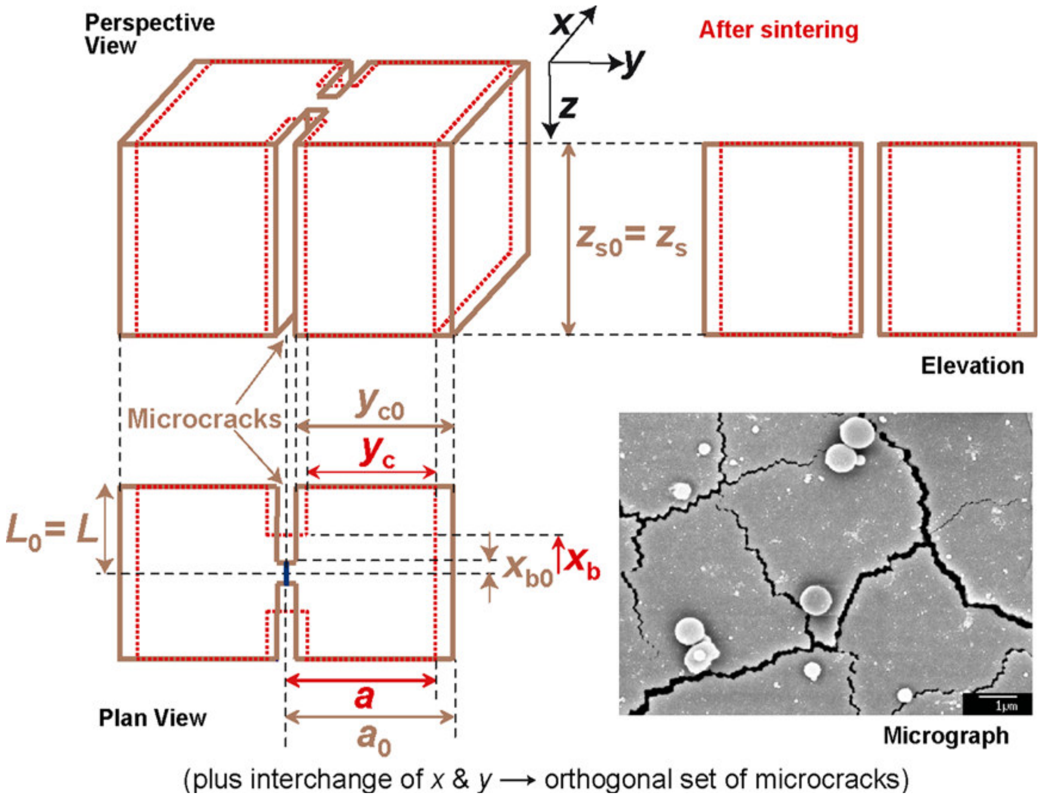

http://dx.doi.org/10.21611/qirt.2012.399

IA characterisation

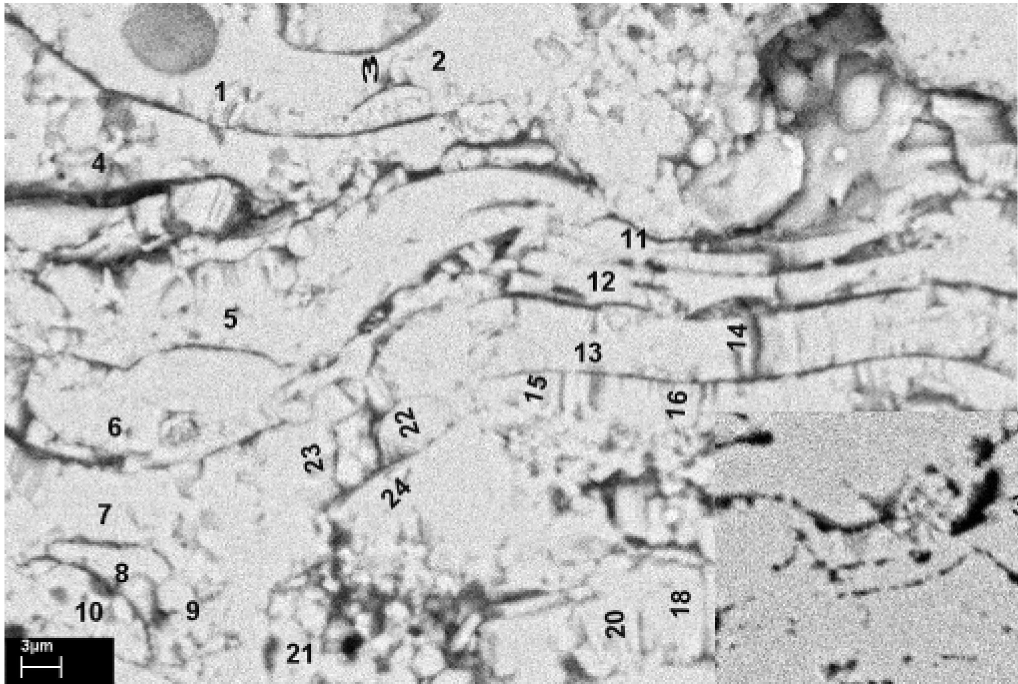

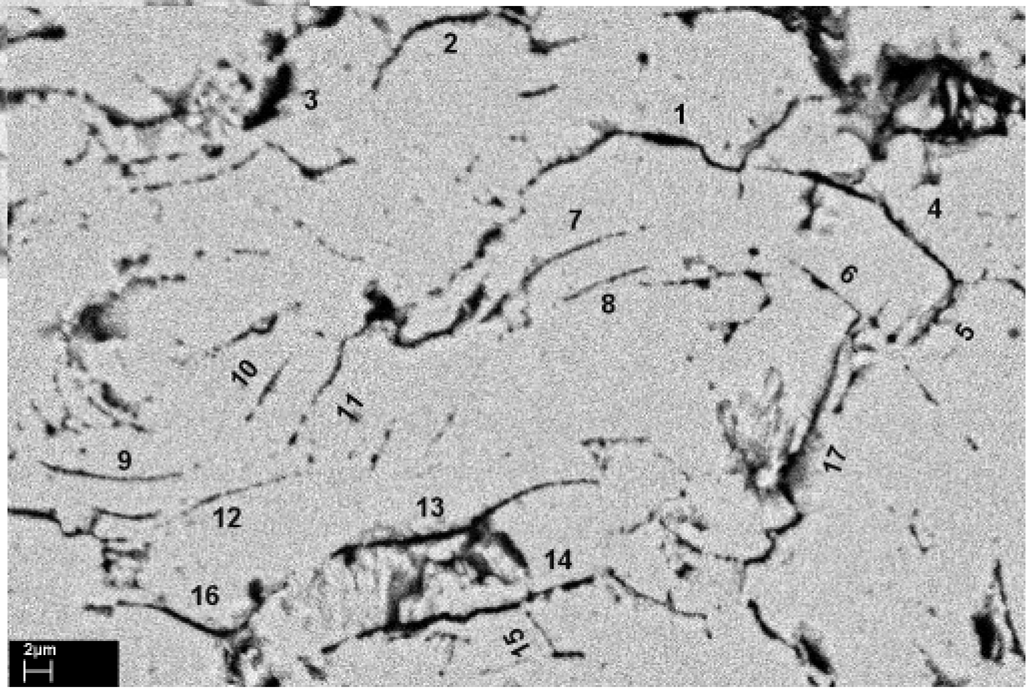

http://dx.doi.org/10.21611/qirt.2012.399

Output of the inversion and sintering codes

WDS1 heat treated

a/c=1/38

a/c=1/22

a/c=1/6

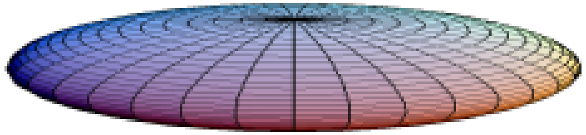

0.088±0.005 μm

0.37±0.05 μm

0.26±0.05 μm

Specific surface area: $1.82 \cdot 10^6$ m^2/m^3

Specific surface area: $1.76 \cdot 10^6$ m^2/m^3

Specific surface area: $0.39 \cdot 10^6$ m^2/m^3

Specific surface area: $0.58 \cdot 10^6$ m^2/m^3

Porosity 10.1

Porosity 8.8

WDS3 heat treated

a/c=1/37

a/c=1/25

a/c=1/14

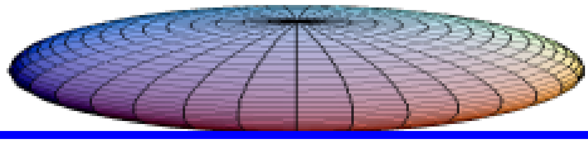

0.163±0.008 μm

0.22±0.05 μm

0.30±0.05 μm

Specific surface area: $0.55 \cdot 10^6$ m^2/m^3

Specific surface area: $0.55 \cdot 10^6$ m^2/m^3

Porosity 13.8

Porosity 12.0

Porosity 10.8

Specific surface area: $0.55 \cdot 10^6$ m^2/m^3

Specific surface area: $0.57 \cdot 10^6$ m^2/m^3

http://dx.doi.org/10.21611/qirt.2012.399

MIP characterisation

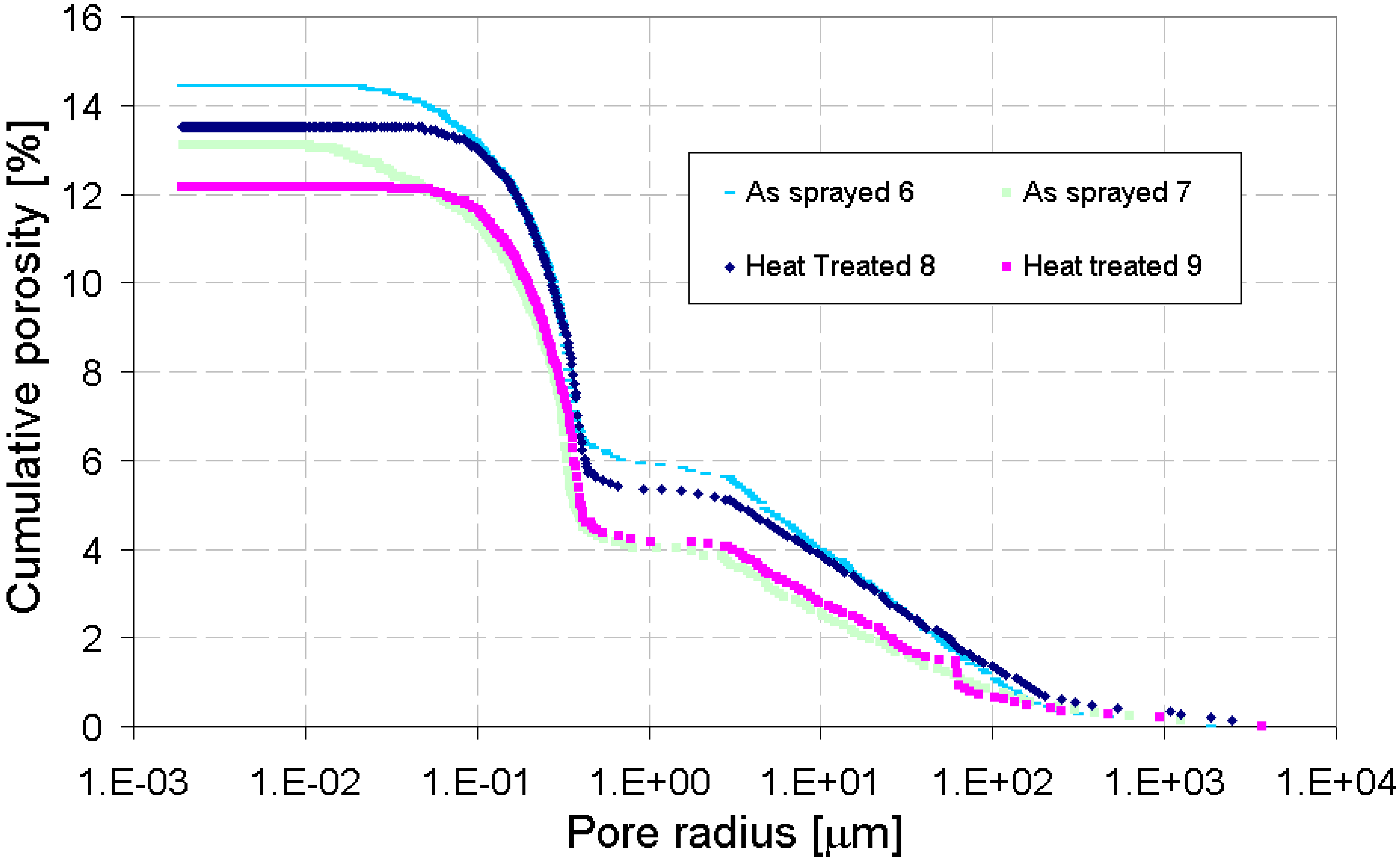

http://dx.doi.org/10.21611/qirt.2012.399

MIP characterisation

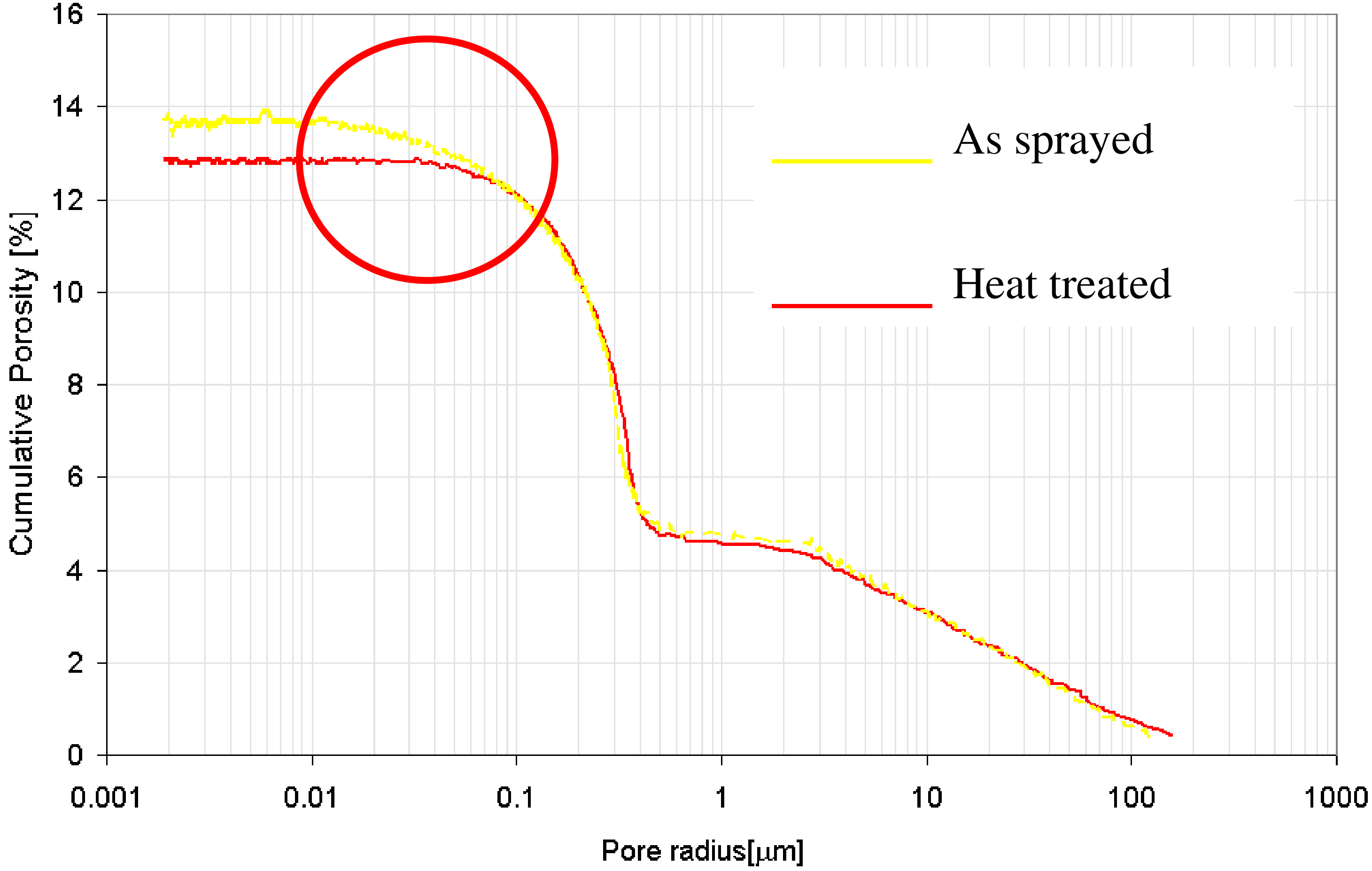

http://dx.doi.org/10.21611/qirt.2012.399

MIP characterisation

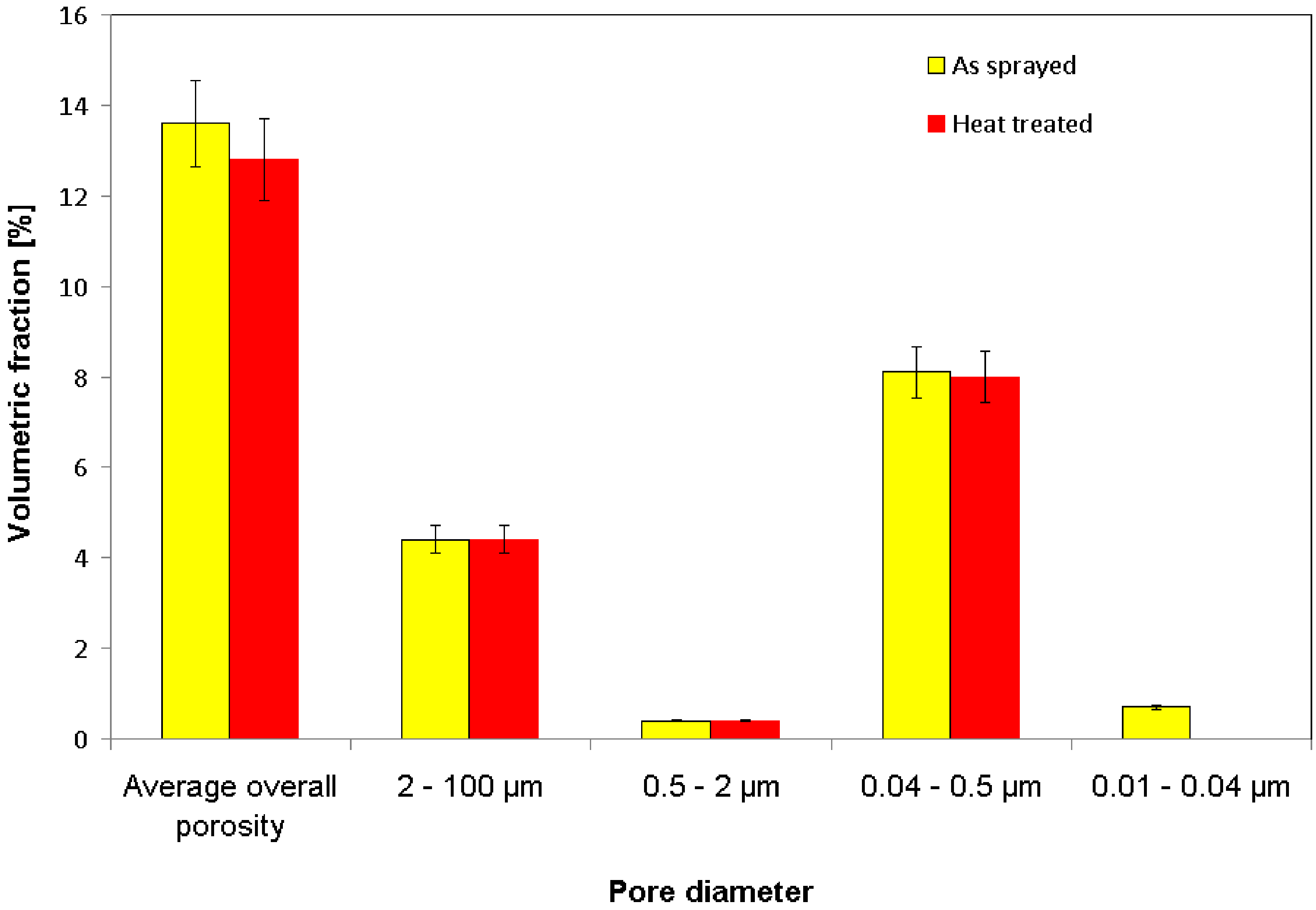

http://dx.doi.org/10.21611/qirt.2012.399

Output of the inversion and sintering codes and MIP

WDS1 heat treated

$a/c=1/38$

$a/c=1/22$

$a/c=1/6$

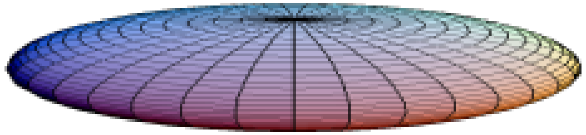

0.088±0.005 μm

0.37±0.05 μm

0.26±0.05 μm

Specific surface area: $1.82 \cdot 10^6$ m^2/m^3

Specific surface area: $0.39 \cdot 10^6$ m^2/m^3

Specific surface area: $0.58 \cdot 10^6$ m^2/m^3

Specific surface area: $0.70 \cdot 10^6$ m^2/m^3

Porosity 10.1

Porosity 8.8

Porosity 13.5

WDS3 heat treated

$a/c=1/37$

$a/c=1/25$

$a/c=1/14$

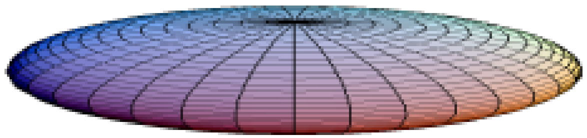

0.163±0.008 μm

0.22±0.05 μm

0.30±0.05 μm

Specific surface area: $0.55 \cdot 10^6$ m^2/m^3

Specific surface area: $0.55 \cdot 10^6$ m^2/m^3

Specific surface area: $0.57 \cdot 10^6$ m^2/m^3

Specific surface area: $0.70 \cdot 10^6$ m^2/m^3

Porosity 12.0

Porosity 10.8

Porosity 12.2

http://dx.doi.org/10.21611/qirt.2012.399

Thermal diffusivity estimations

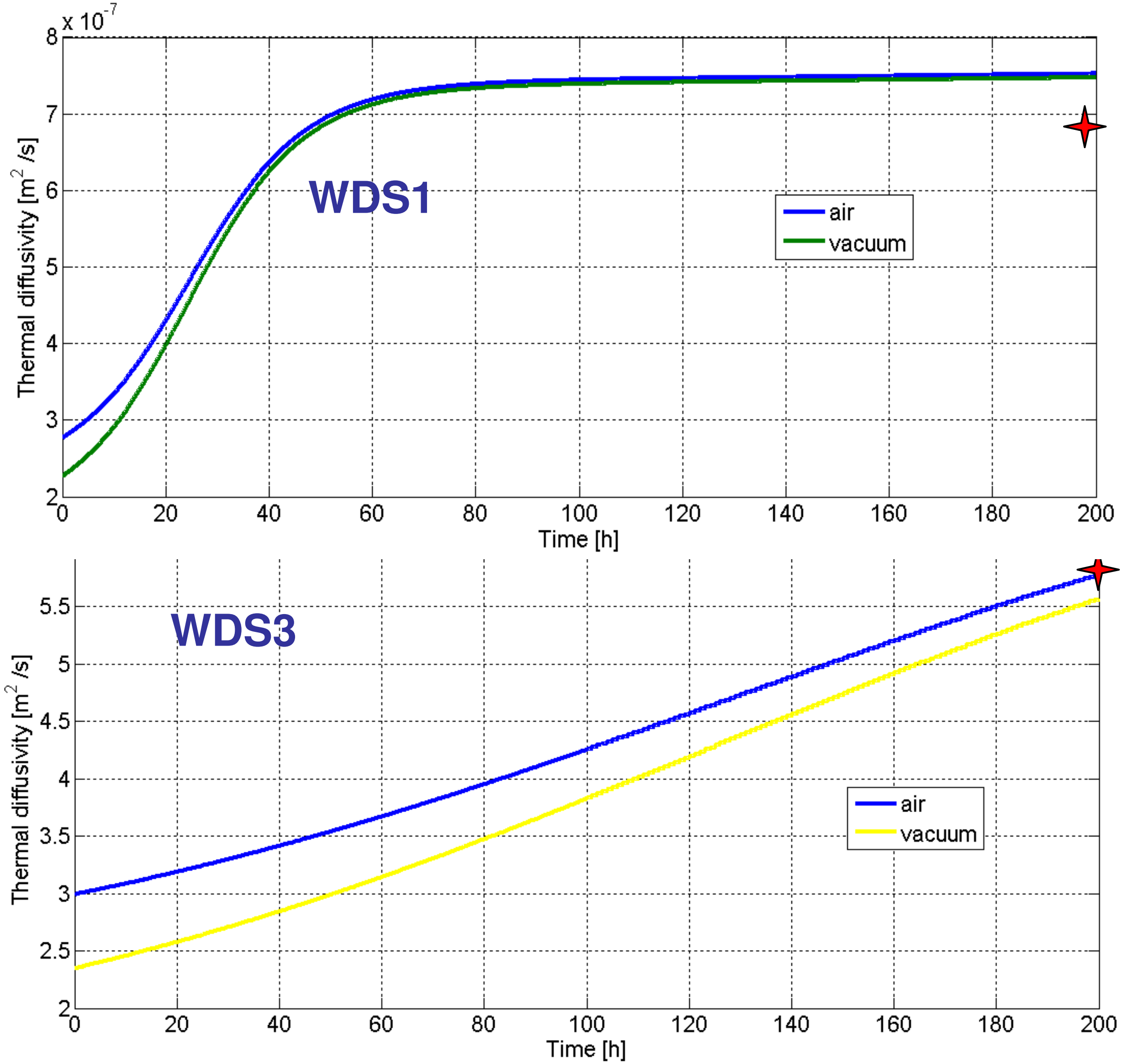

http://dx.doi.org/10.21611/qirt.2012.399

Conclusive remarks

✓A good agreement between the experimental estimations of **specific surface area** by MIP, Inversion code and Sintering model has been found

✓The effective **crack opening** estimated by the inversion code is in good agreement with sintering model and IA

✓**Aspect ratios increase** as estimated by inversion code only partially agrees with that forecasted by the sintering code

✓**Porosity drop** as measured by MIP resulted smaller than that observed by IA and forecasted by sintering model

✓**Thermal diffusivity** forecasts in ”good” agreement with experimental results for one heat treated sample. A bimodal fine pore distribution could be a possible explanation for the overestimation of thermal diffusivity for sample 1

✓Thermal diffusivity measurements using different gases and pressures coupled with IA seems to be a useful technique to obtain microstructural parameters to be used as input for the sintering model

http://dx.doi.org/10.21611/qirt.2012.399

Through-the-thickness and in-plane thermal diffusivity measurements

http://dx.doi.org/10.21611/qirt.2012.399

Laser thermography

In-plane thermal diffusivity

$$\frac{\Theta(k,z,t)}{\Theta(k=0,z,t)} = \frac{F(k)}{F(k=0)} e^{-\alpha_p k^2 t}$$

For slab or semi-infinite body, the spatial Fourier Transform Θ of the in-plane temperature field, decays exponentially in time once normalized by its continuous component. Hence, taking the logarithm of the ratio, it is possible to obtain the in-plane diffusivity from the slope of the fitting straight line.

http://dx.doi.org/10.21611/qirt.2012.399

Laser thermography

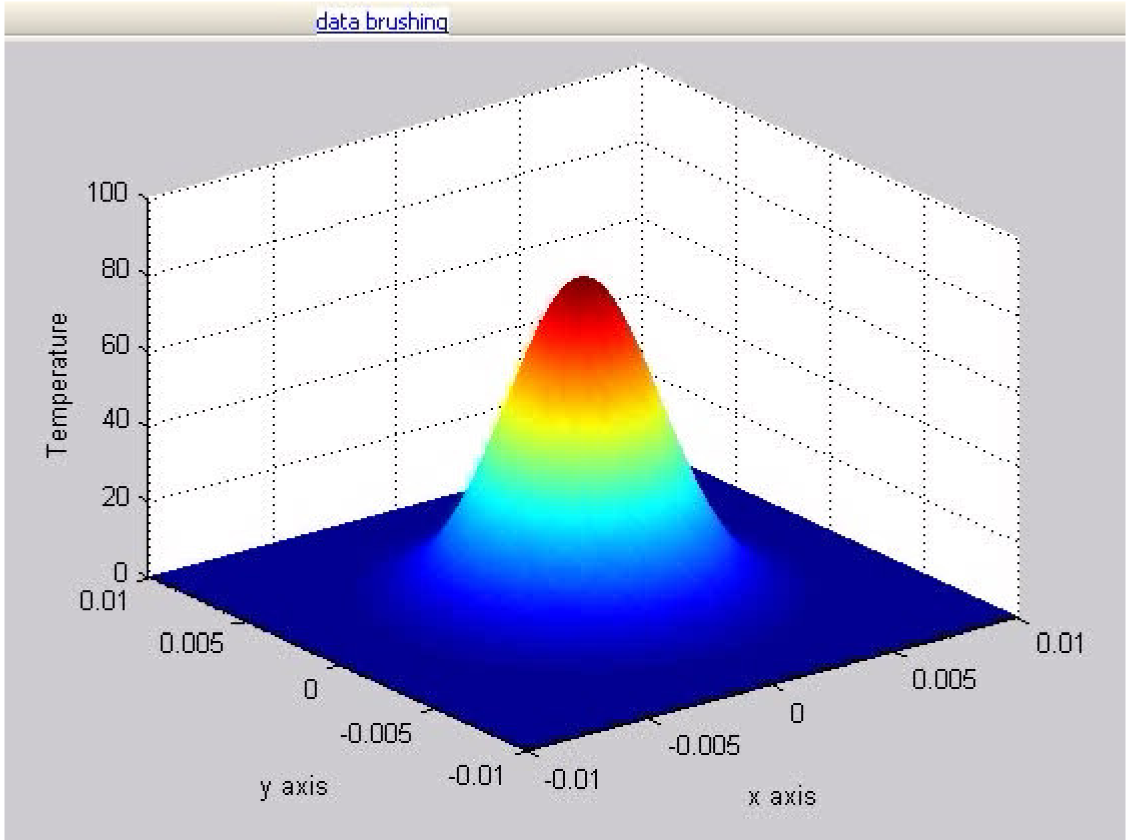

F. Cernuschi, A. Russo, L. Lorenzoni, A. Figari, *Review of Scientific Instruments* Vol. 72 (10), 2001, p. 1-8.

P. Bison, F. Cernuschi, S. Capelli, *Surf. Coat Technol*. Vol. 205, Issue 10, 2011, Pag..3128-3133.

http://dx.doi.org/10.21611/qirt.2012.399

Laser thermography

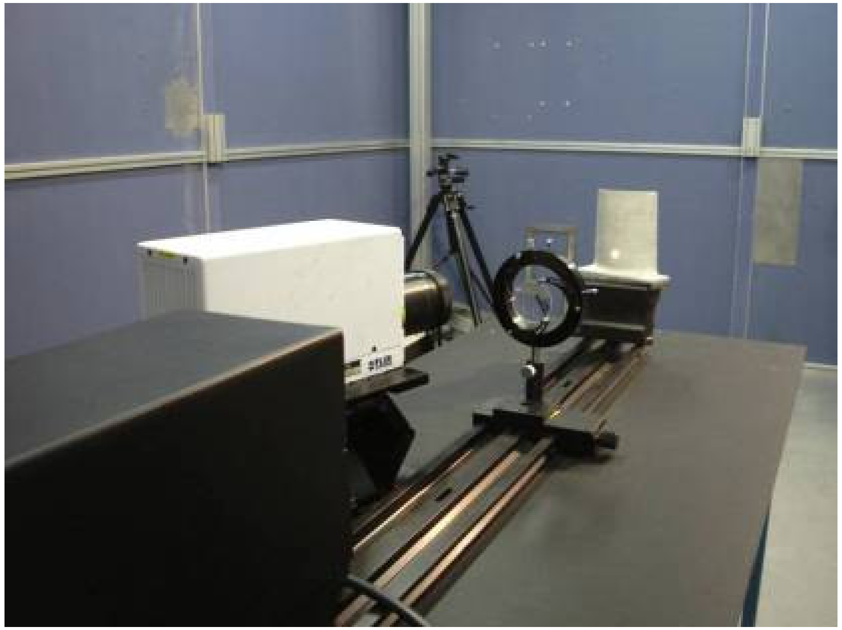

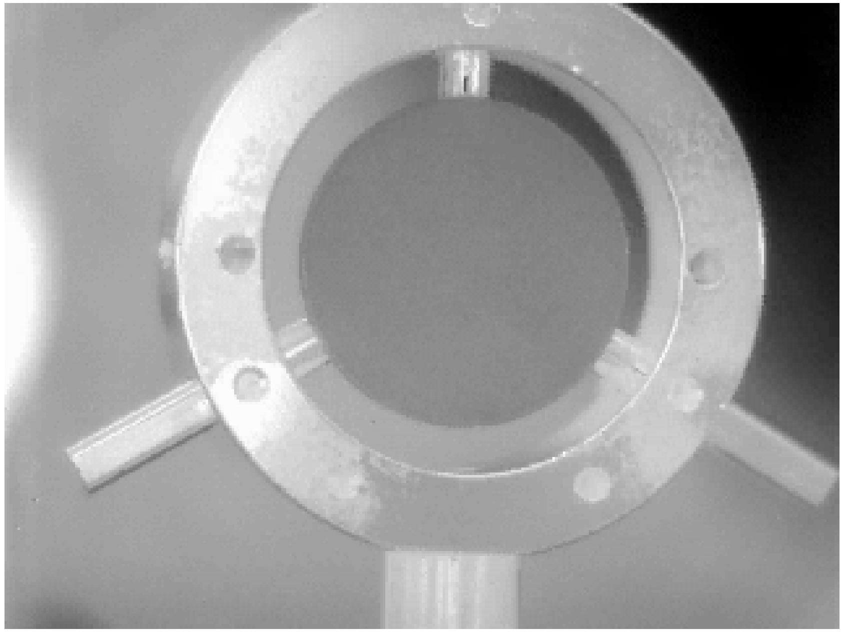

P.G. Bison, F. Cernuschi, E. Grinzato, S. Marinetti, D. Robba, *Infrared Physics and Technology*, 49 (2007) 286.

http://dx.doi.org/10.21611/qirt.2012.399

Laser thermography - in-plane thermal diffusivity

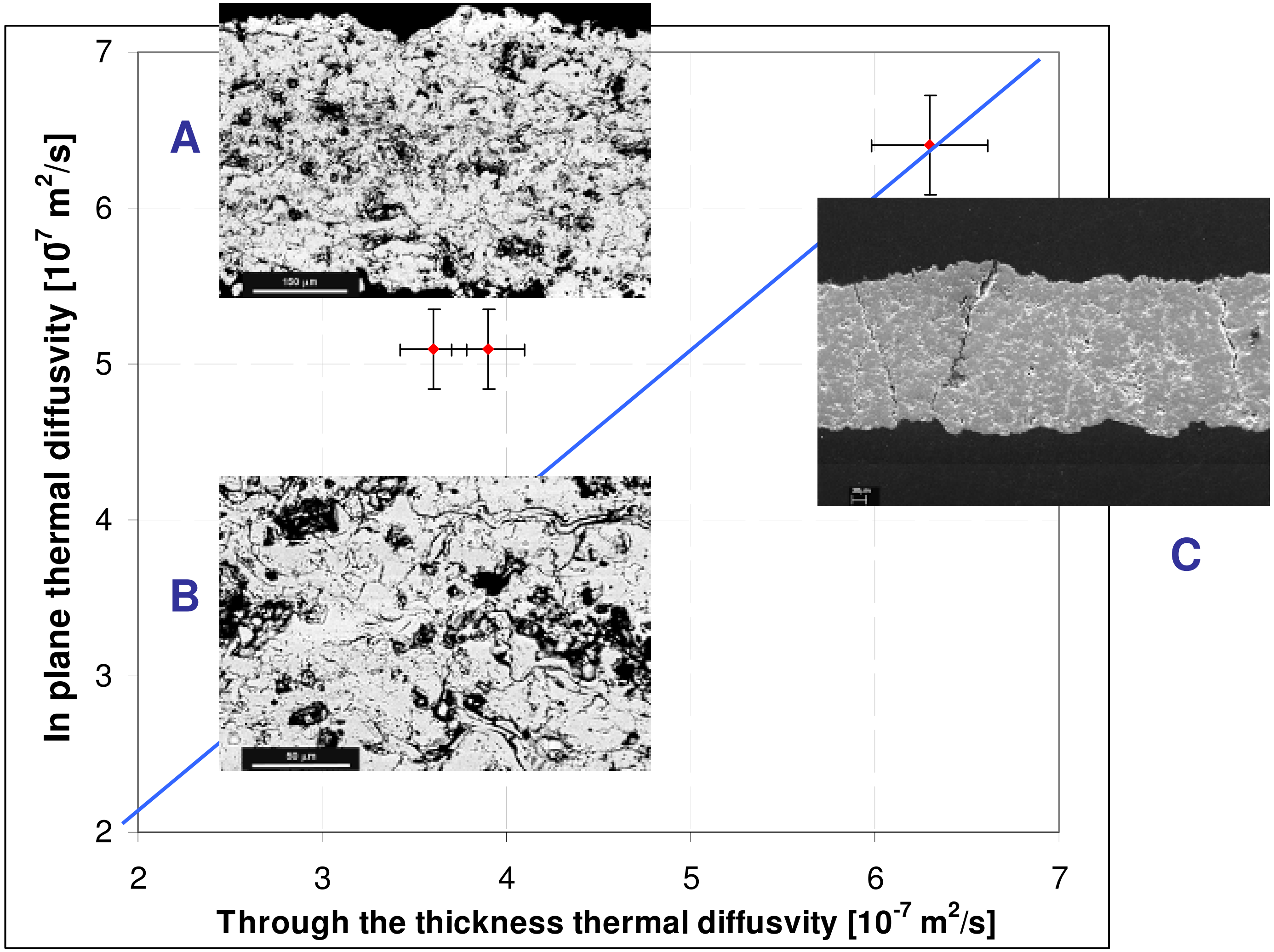

P. Bison, F. Cernuschi, S. Capelli, *Surf. Coat Technol*. Vol. 205, Issue 10, 2011, Pag..3128-3133.

http://dx.doi.org/10.21611/qirt.2012.399

Laser thermography - in-plane thermal diffusivity

Elastic modulus measured by three point bending test

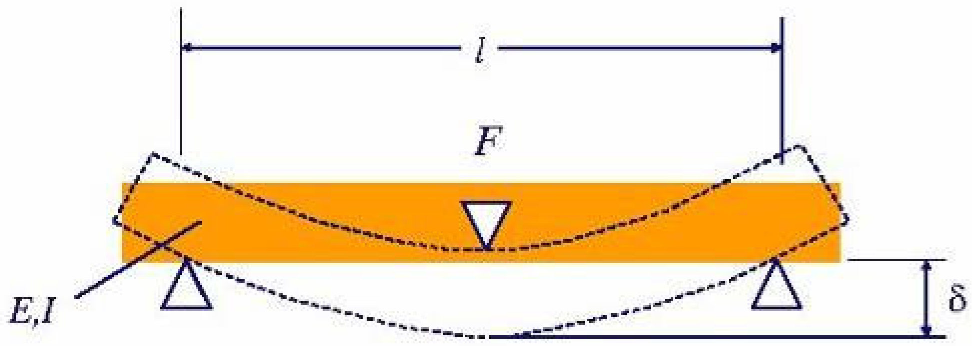

$$\sigma = \frac{\pm Fl}{4I} y \qquad \delta = \frac{Fl^3}{48EI}$$

Sample	In-depth thermal diffusivity [10^{-7} m^2 s^{-1}]	In depth thermal conductivity [W/ mK]	In-plane thermal diffusivity [10^{-7} m^2 s^{-1}]	In-plane thermal conductivity [W/ mK]	In-plane elastic modulus E [GPa]	Simulated in-depth Thermal diffusivity [10^{-7} m^2 s^{-1}]
A	3.6±0.3	0.8	5.1±0.4	1.1	9.5±0.8	2.8
B	3.9±0.4	0.9	5.1±0.4	1.2	11.4±1.5	3.9
C	6.3±0.1	1.6	6.4±0.2	1.6	1.8±1.5	6.7

http://dx.doi.org/10.21611/qirt.2012.399

Laser thermography - in-plane thermal diffusivity

In the literature several correlations between mechanical and thermo-physical properties of heterogeneous solids have been proposed. It is worth comparing in our case the *in-plane* thermal diffusivity and the *in-plane* elastic modulus of the three samples.

$$\alpha_{pA} / \alpha_{pB} \cong E_A / E_B$$

$$\alpha_{pA} / \alpha_{pC} \cong \alpha_{pB} / \alpha_{pC} << E_A / E_C \cong E_B / E_C$$

The assumptions underneath the cross correlation models usually the porosity is supposed to be some orders of magnitude smaller than the typical TBC thickness. In the case of vertical cracks crossing most of TBC thickness this is not true anymore.

http://dx.doi.org/10.21611/qirt.2012.399

Thank you for your kind attention!